Dyes and Pigments 251 (2026) 113696

Contents lists available at ScienceDirect

Dyes and Pigments

journal homepage: www.elsevier.com/locate/dyepig

Chromogenic azomacrocycles with imidazole residue – Part II: Effect of spacer type and N–H orientation on chromogenic and spectroscopic properties

Paulina Miklaszewska [a], Michał Aszyk [a], Paweł Sowiński [b], Andrzej Okuniewski [c], Zofia Kaczorowska [a], Zuzanna Antonowicz [a], Gabriela Burakowska [a], Ewa Wagner-Wysiecka [a,d,*]

[a] Department of Chemistry and Technology of Functional Materials, Faculty of Chemistry, Gdańsk University of Technology, Narutowicza Street 11/12, 80-233, Gdańsk, Poland
[b] Nuclear Magnetic Resonance Laboratory, Faculty of Chemistry, Gdańsk University of Technology, Narutowicza Street 11/12, 80-233, Gdańsk, Poland
[c] Department of Inorganic Chemistry, Faculty of Chemistry, Gdańsk University of Technology, Narutowicza Street 11/12, 80-233, Gdańsk, Poland
[d] Advanced Materials Center, Department of Chemistry, Gdańsk University of Technology, Narutowicza Street 11/12, 80-233, Gdańsk, Poland

ARTICLE INFO

Keywords:
Supramolecular chemistry
Azomacrocycles
Imidazole-based chromoionophores
Metal ion recognition
Colorimetric sensors

ABSTRACT

Building upon our previous studies on imidazole-based chromogenic azomacrocycles, a novel 17-membered bisazomacrocycle bearing 2-methylimidazole, **5C2MeIm**, was synthesised and compared with its 17-membered oligoether-linked analogue **3O2MeIm**. Macrocyclisation was more efficient for the oligoether-linked compound, while the use of cyclodextrins as molecular reactors had no significant effect on the yield of hydrocarbon-linked macrocycle.The chromogenic and binding behaviour of **5C2MeIm** and **3O2MeIm** towards Pb(II) and Cu(II) was evaluated by digital colour analysis and UV-Vis spectrophotometry. Predominantly, 2:1 sandwich-type complexes with Pb(II) were formed, although 3:2 triple-decker species were also detected. FTIR data indicated distinct coordination modes for both cations. Receptor layers incorporating **3O2MeIm** and **5C2MeIm**, exhibited low selectivity towards metal cations.

These results demonstrate that subtle structural variations, such as the position of the methyl substituent affecting macrocycle size and the orientation of the N–H group within the macrocyclic cavity, markedly influence chromogenic and complexation behaviour. Understanding these effects provides valuable insight into the design principles governing chromoionophores and their metal ion recognition behaviour.

1. Introduction

Heavy metals are defined as metals or metalloids characterised by high density [1], which can cause adverse effects even at low concentrations [1,2]. The pollution of soil and water with heavy metals is a problem that appears to be increasingly relevant these days. The intensive development of heavy industries can causeanincrease in concentrations of heavy metals in natural environment [3–5]. However, while the anthropogenic factor cannot be omitted in this discussion, it is important to notice that these metal scan be introduced to the ecosystem following natural processes such as volcanic eruptions or forest fires [5]. The abundance of heavy metals in the environment and their non-biodegradability cause these pollutants to be a threat for aquatic and land flora and fauna, and, consequently, for humans [3–8]. It has been reported that the most common metals that induce severe effects are mercury, lead, chromium, cadmium and arsenic [9,10]. It needs to be addressed, however, that some heavy metals, such as copper [11] or zinc [12], although necessary for maintaining homeostasis in human body, can be considered pollutants as well. Copper is a microelement that is essential for various organisms to function properly [13]. It participates in, among others, the production of erythrocytes [14], collagen [15,16] and elastin fibres [16] or in modulation of signal pathways in human cells [17]. The deficiency of copper can be associated in some cases with: anaemia [18,19], cytopaenia [19,20] or

* Corresponding author. Department of Chemistry and Technology of Functional Materials, Faculty of Chemistry, Gdańsk University of Technology, Narutowicza Street 11/12, 80-233, Gdańsk, Poland.
E-mail address: ewa.wagner-wysiecka@pg.edu.pl (E. Wagner-Wysiecka).

https://doi.org/10.1016/j.dyepig.2026.113696
Received 5 October 2025; Received in revised form 27 February 2026; Accepted 4 March 2026
Available online 4 March 2026

myelopathy [19]. While a certain amount of copper is necessary for humans, exposure to larger quantities of copper can lead to different toxic effects. A link between copper ion excess and carcinogenesis has been reported by various authors [21–23]. Increased levels of copper in the body may also cause neural pathologies such as memory loss due to the accumulation of copper in parts of the brain [24]. It is therefore crucial to closely monitor levels of copper intake, especially for people affected by Wilson or Menkes disease, which disrupt metabolism of this element [25].

Unlike copper, lead is a strictly toxic element for human body. It is capable of accumulating in various tissues, with the vast majority of it being mineralised tissues, such as bones and teeth [26]. Lead can permanently affect, among others, nervous [27], cardiovascular [28] and respiratory [29] system, which in turn can even lead to death. WHO estimates that in 2019 almost 50% of 2 million deaths that occurred due to chemical exposure were caused by lead [30].

In recent years, the interest in the detrimental health effects of heavy metal presence in food has increased [31]. Therefore it is crucial to develop sensors that would be able to determine and identify the content of heavy metal cations in environmental and biological samples. There are various approaches to the subject, including electrochemical sensors [32] and biosensors [33,34]. However, due to low costs of production and fast response time, increasingly more optical sensors are being developed [35]. In optical sensors, chromoionophoric compounds are often immobilised on porous materials [36–38] or in polymeric matrices [39–41]. Aside from high sensitivity to the analyte, they are characterised by their simplicity: the measurement requires no specialised equipment to be accurately performed. Selective chromoionophores can also serve as components of ion-selective membranes for metal cations detection and/or removal e.g. from wastewaters or environmental samples [42–44]. In this regard macrocyclic chromoionophores, due to their constitutional features, seem to be particularly interesting. In our research group we have obtained chromoionophoric macrocyclic azocompounds bearing pyrrole and imidazole moieties that displayed selectivity towards heavy metal cations, such as bismuth [45], copper [46] and lead [45,47–49]. In particular, pyrrole-based diazocrowns were shown to form well-defined 3:2 ligand-Pb(II) complexes in acetonitrile, with intense and well-resolved ESI-MS signals consistent with triple-decker species, and were successfully applied as chromoionophores in optical Pb(II) sensors [47,48].

Building upon our earlier findings on chromogenic azomacrocycles with imidazole residues [37,48], this study extends the series by systematically analysing how subtle structural modifications—specifically, the position of the methyl substituent in the imidazole ring, which determines the direction of the coupling reaction and thus the macrocycle size and the orientation of the N–H group within the macrocyclic cavity—influence chromogenic and ion-binding behaviour. These effects have not been previously discussed in the context of azomacrocyclic chromoionophores, and are essential for understanding the structure–property relationship governing their sensing performance.

2. Experimental

2.1. Materials

All chemicals of the highest available purity were purchased from commercial sources and used without further purification. Metal perchlorates: lithium perchlorate (99.9%, Sigma Aldrich), sodium perchlorate monohydrate (>99.0%, Fluka), potassium perchlorate (>99.0%, Sigma Aldrich), magnesium perchlorate (≤100%, Alfa Aesar), calcium perchlorate tetrahydrate (99.0%, Alfa Aesar), strontium perchlorate trihydrate (≤100%, Alfa Aesar), barium perchlorate (97.0%, Sigma Aldrich), cobalt(II) perchlorate hexahydrate (98.0%, Sigma Aldrich), nickel(II) perchlorate hexahydrate (≥98.5%, Sigma Aldrich), copper(II) perchlorate hexahydrate (98.0%, Sigma Aldrich), zinc perchlorate hexahydrate (Sigma Aldrich), cadmium perchlorate hexahydrate (Alfa Aesar) and lead(II) perchlorate trihydrate (≥99.0%, Sigma Aldrich). Metal nitrates: sodium nitrate (≥99.8%, POCH), potassium nitrate (≥99.8%, POCH), magnesium nitrate hexahydrate (≥99.0%, POCH), calcium nitrate tetrahydrate (≥99.0%, POCH), strontium nitrate (≥99.0%, POCH), barium nitrate (≥99.0%, POCH), cobalt(II) nitrate hexahydrate (≥98.0%, POCH), nickel(II) nitrate hexahydrate (≥98.0%, POCH), copper(II) nitrate trihydrate (≥99.5%, Merck), zinc nitrate hexahydrate (≥98.0%, POCH), cadmium nitrate tetrahydrate (≥98.0%, POCH),lead(II) nitrate (≥99.0%, Alfa Aesar)and bismuth(III) nitrate pentahydrate (≥98.0%, Sigma Aldrich). Nitric acid (65%, p.a., POCh). Copper chloride dihydrate (p.a., POCH). Disodium EDTA (p.a., POCH). Tris(hydroxymethyl)aminomethane (TRIS) was purchased from Serva.

Porous glass (polystyrene modified, particle size 0.075–0.125 mm, Mw ~ 120000 Corning) and cellulose powder (Merck) were used for preparation of sensing layers. Cellulose triacetate (CTA) was acquired from Acros Organics. Triethyleneglycol ≥99.0% (TEG) was obtained from Merck. Bis(2-ethylhexyl) phthalate ≥99.5% (DOP), bis(2-ethylhexyl) sebacate ≥97.0% (DOS) and 2-nitrophenyl octyl ether ≥99.0% (NPOE) were purchased from Sigma Aldrich (Selectophore). Cyclodextrins: α-CD and γ-CD (TCI Europe, Belgium), β-CD (Fluka, Sigma–Aldrich, Germany) were used as purchased. UV–Vis measurements were carried out in acetonitrile (spectroscopic-grade, Merck) and DMSO (POCh). All aqueous solutions were prepared using ultra-pure water obtained by the reverse osmosis (RO) from Hydrolab Poland station (conductivity <1 μS/cm^{-1}). In synthetic protocols p.a. solvents were used. Chromatography: TLC plates 60 RP-18 F_{254} for lipophilicity determination, TLC plates 60 F_{254} for reaction progress tracing and determination of R_f parameters and silica gel 60 (0.063 - 0.200 mm) for column chromatography were purchased from Merck.

2.2. Instrumentation

^{1}H NMR and ^{13}C NMR spectra were registered on Varian INOVA 500 spectrometer at 500 MHz and 125 MHz, respectively. Two-dimensional NMR experiments were performed on the same instrument. The ROESYAD experiment (standard Varian library sequence) was carried out with a spinlock mixing time of 0.3 s, relaxation delay (d1) of 1.4 s and acquisition time (at) of 0.35 s. DOSY spectra were acquired using the standard Varian Dbppste_cc pulse sequence with a maximum gradient strength of 27261 (Performa II/III), diffusion gradient length of 3 ms and diffusion delay of 100 ms. FTIR spectra (ATR) were taken on the Nicolet iS10 apparatus. Mass spectra (HRMS ESI) were recorded on Autospec Premier (Waters) spectrometer. UV–Vis measurements were carried out in 1 cm quartz cuvettes with the use of UNICAM UV 300 series spectrometer. Portable LED light box (23 × 23 × 23 cm) was used to guarantee the reproducibility of the photos (PULUZ, Photography Light Box, Shenzhen Puluz Technology Limited). The photos were taken with Apple iPhone 14.

2.3. Synthesis of macrocycles

Macrocycle **3O2MeIm** was obtained according to previously described procedure [50]. The identity of the compound was confirmed by comparison of spectroscopic characteristics (^{1}H NMR, FTIR) and chromatographic properties of compound with a sample of the genuine **3O2MeIm** deposited in our lab. New macrocycle, **5C2MeIm**, was obtained in analogous way, namely by coupling 2-methylimidazole with the bis-diazonium salt under high dilution conditions (pH 10, NaOH) [37,50]. Substrates, namely dinitropodand (compound 1, Scheme 1) and diamine (compound 2, Scheme 1), were obtained as described previously [37].

Two solutions were prepared:

- Solution A: Bis-amine (2 mmol) was dissolved in 40 ml pre-cooled water and acidified with conc. hydrochloric acid (1 ml). The

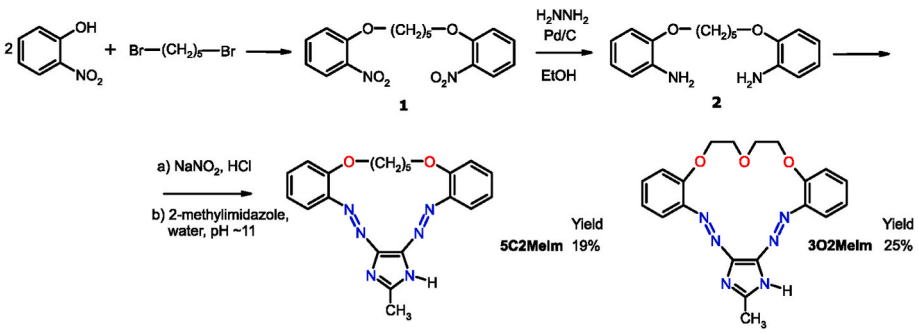

Scheme 1. Synthetic route for new 2-methylimidazole bearing azomacrocycle **5C2MeIm**; yield of oligoether analogue **3O2MeIm** [50].

solution was diazotised with sodium nitrite (4.4 mmol) dissolved in cold water (2 ml).

- Solution B: 2-methylimidazole (2 mmol) and sodium hydroxide (5 mmol) were dissolved in ice-cooled water (40 ml).

All solutions were cooled in an ice bath to 0–5 °C. After this time, solutions: A (bisdiazonium salt) and B were added dropwise to deionized water (600 mL) at pH ~10 (NaOH) within 30 min, ensuring intensive stirring of the reaction system. The pH was controlled during the addition of solutions to the reaction container. After 2 h, the ice bath was removed, and the mixture was vigorously stirred for 24 h at room temperature. The precipitate was filtered off under reduced pressure. Product was isolated by column chromatography using initially dichloromethane and finally dichloromethane:acetone (100:1; 50:1; 20:5; 10:1 v/v) as eluent.

The effect of CDs on the reaction yield: equimolar amounts of α-, β-, and γ -cyclodextrins were added to the solution of 2-methylimidazole. Then diazocoupling was carried out in the same way as described above.

The structure of **5C2MeIm** was confirmed by spectroscopic methods. The obtained spectra are shown in Supplementary Material, Fig. S1.

5C2MeIm, red solid, yield 19%, mp 194-196 °C, $R_f = 0.29$ ($CHCl_3$: MeOH 20:1, v/v), **FTIR** (ATR) [cm^{-1}]: 3064; 2933; 2867; 2752; 2636; 1593; 1570; 1557; 1526; 1488; 1464; 1448; 1387; 1278; 1245; 1160; 1116; 1047; 953; 941; 752; 566. **^{1}H NMR** (DMSO-d_6, 500 MHz), δ[ppm]: 1.60-1.80 (m, 6H); 2.48 (s, 3H); 3.99 (s, 4H); 7.08-7.16 (m, 2H); 7.34 (t, $J = 8.1$ Hz, 2H); 7.58-7.62 (m, 2H); 12.92 (s, ~1H). **^{13}C NMR** (DMSO-d_6, 125 MHz), δ [ppm]:150.35, 149.50, 149.22, 148.21, 143.68, 142.21, 130.90, 129.32, 129.21, 120.62, 113.62, 68.27, 68.11, 29.11, 24.08, 14.81. **HRMS (ESI)** *m/z* $[M+H]^+$ calc. for $C_{21}H_{23}N_6O_2$ 391.1882; found 391.1885.

UV-Vis characterisation of **5C2MeIm** and **3O2MeIm** is presented in Table S1.

2.4. Lipophilicity

Lipophilicity of investigated compounds was determined by reversed-phase thin layer chromatography method [37,51]. RP-18 plates were developed in the methanol:water and methanol:acetic acid system (9:1, v/v). As reference, DOS, DOP and *o*-NPOE were developed along with the macrocycle samples.

2.5. Metal cation complexation

2.5.1. Stability constants determination

Metal cation complexation was investigated in DMSO, acetonitrile and mixture of these solvents with water (9:1, v/v). For qualitative tests the stock solutions (10 mL flasks) of macrocycles were prepared by weighting the respective amount of azocrowns. Metal salts were added in excess (by addition of solid salt).

UV-Vis spectroscopy was used to investigate the copper(II) and lead (II) cation binding abilities of **5C2MeIm** and **3O2MeIm** and to calculate the stability constants of formed complexes. The complexation studies were carried out in DMSO:water (9:1, v/v) and acetonitrile:water (9:1, v/v) systems. Stock solutions of **5C2MeIm** (c ~10^{-3} M), **3O2MeIm** (c ~10^{-3} M), copper(II) nitrate (c ~10^{-3} M), lead(II) nitrate (c ~10^{-3} M), copper(II) perchlorate (c ~10^{-3} M), and lead(II) perchlorate (c ~10^{-3} M) were prepared by weighting the respective compounds, dissolving the compounds in organic solvents in volumetric flasks, and then adding water in adequate proportions. In order to register the spectrum, 100 μl of **5C2MeIm** or 70 μl of **3O2MeIm** was transferred to quartz cuvette and diluted with the respective system until the total volume of the solution in the cuvette reached 2.4 mL. Investigated compounds were titrated with nitrate and perchlorate solutions. For stability constant calculations, OPIUM software was used [52]. Stoichiometry of the complexes formed under titration experiment conditions was analysed by Job's method.

2.5.2. Counter-ion effect

To assess the influence of counter-anions on metal–ligand complexation equilibria and spectral response, additional UV–Vis titration experiments were performed using chloride and nitrate salts of Cu(II) and Pb(II) in acetonitrile:water (9:1, v/v).

Stock solutions of $CuCl_2{\cdot}2H_2O$, $Cu(NO_3)_2{\cdot}3H_2O$ and $Pb(NO_3)_2$ were prepared under the same concentration conditions as applied in the primary titration experiments conducted with perchlorate salts. The titrations of **5C2MeIm** and **3O2MeIm** were performed analogously to the procedure described above.

2.5.3. Competition (interfering ion) experiments

To evaluate the susceptibility of the metal–ligand systems toward competitive metal ions, competition experiments were performed using UV–Vis spectrophotometry in acetonitrile:water (9:1, v/v).

In a typical procedure, a solution of **5C2MeIm** or **3O2MeIm** was first treated with copper(II) perchlorate or lead(II) perchlorate at a concentration sufficient to reach the limiting spectrum corresponding to the endpoint observed in the primary spectrophotometric titration experiments (i.e., a reproducible "metal-saturated" metal–ligand complex state). The resulting solution was subsequently titrated with a solution of a competing metal ion (Zn(II), Ni(II), Cu(II), or Pb(II), as perchlorate salts), depending on the system under investigation.

UV–Vis spectra were recorded after each addition under identical instrumental conditions as applied in the primary titration experiments. Changes in absorbance at characteristic wavelengths were monitored throughout the titration. The extent of interference was quantified using the Relative Response Percentage (RR%), calculated from the change in absorbance (ΔA) relative to the response induced by the primary metal ion under identical conditions.

2.5.4. Metal ion complexation in ^{1}H NMR and FTIR studies

For ^{1}H NMR experiments the weighted amount of respective crowns was prepared. After dissolution in acetonitrile-d_3, weighted amount of lead(II) perchlorate were added to obtain 2:1 (crown:lead(II)) and 1:5

(crown:lead(II)) molar ratio.

For FTIR experiments, a series of weightings were prepared to obtain desired molar ratios. The contents of vials were dissolved in methanol and left for evaporation. Spectra of free crowns **3O2MeIm** and **5C2MeIm,** as well as their complexes, were analysed in solid state.

2.6. Effect of acidity of solvent on colorimetric response

The investigation of colorimetric response under varying acidity conditions was conducted in acetonitrile/aqueous HNO_3 (1:1, v/v; c $(HNO_3) = 10^{-3}$ M in the aqueous phase) and acetonitrile/aqueous TRIS (1:1, v/v; c(TRIS) = 1.0 M in the aqueous phase) systems. $Cu(NO_3)_2$ ($c = 5.5{\cdot}10^{-2}$ M) and $Pb(NO_3)_2$ ($c = 2.8{\cdot}10^{-2}$ M) were added to the solutions of **5C2MeIm** ($5.6{\cdot}10^{-5}$ M) and **3O2MeIm** ($2.7{\cdot}10^{-5}$ M) in a 1:4 (ligand: salt) molar ratio.

In the presence of Pb(II) salt, the studies could not be performed in the TRIS-containing medium due to the formation of insoluble Pb(II) hydrolysis products in non-acidic conditions [53,54]. The optical response of the ligands in the presence of metal salts was analysed by UV–Vis spectroscopy.

2.7. Preparation of sensing layers and their regeneration

The procedure for preparing the CTA membranes was as follows: chromoionophore (1 mg), together with cellulose triacetate (250 mg) and ethylene glycol (150 μl), were dissolved in dichloromethane (6 ml). The entire mixture was stirred on a magnetic stirrer, and the obtained solution was then spread evenly onto a 9 cm diameter Petri dish and left until the solvent evaporated completely. The membranes were successively cut into 0.9 × 4.5 cm strips.

Cellulose or polystyrene modified glass (PG-PS) sensing materials with respective chromoionophore were prepared using 1 mg/10 mL of chromoionophore working solution. Then 5 mL of the stock solution was taken sequentially and diluted to 10 mL with dichloromethane. To the thus obtained solution, 500 mg of cellulose or PG-PS was added to obtain sensor materials with chromoionophore contents of 1 mg/g of solid material. The mixture was stirred with a magnetic stirrer for 10 min and then transferred evenly to a Petri dish and left until the solvent evaporated completely. The properties of receptor layers with a concentration of 1 mg/g of solid material were studied after immobilisation of the resulting material with double-sided tape on 0.9 × 4.5 cm glass plates. Metal nitrate solutions for study of the properties of the receptor layers were prepared in nitric acid solution (10^{-3} M), while 0.1 M sodium hydroxide and nitric acid aqueous solutions were used as base and acid.

Regeneration properties of receptor layers were investigated by exposing the metal-loaded films to disodium EDTA (0.1 M) and HNO_3 (0.1 M) solutions. The receptor layers were first immersed in $Cu(NO_3)_2$ or $Pb(NO_3)_2$ solutions (0.1 M) for 10 min. Following this, the films were treated with regenerative solutions: HNO_3 for 10 min and EDTA for 30 min. Afterwards, the films were washed three times with deionized water to remove any residual metal salts and regenerative agents. The optical response of the films was monitored over five cycles for CTA-based optodes and one cycle for PG-PS-based sensors. The regeneration process was documented by measuring the colorimetric response at each cycle, as presented in the Results section.

2.8. Digital colour analysis

For the editing and processing of the images (photos of solutions and receptor layers) free software ImageJ [55] was used. The colour image was split into three channels (R, G, and B) and the intensity of each channel was recorded separately as a text file. The colour intensity (I), represented in the RGB images, was expressed as [56]:

$$I = 0.299R + 0.587G + 0.114B$$

Parameter I closely represents the average person's relative perception of the brightness of red, green, and blue light. For comparison, parameter I_A, which is the average value of the three components (red, green, and blue) as the greyscale value was used as follows:

$$I_A = \frac{(R + G + B)}{3}$$

In order to determine the change in colour, given as ΔE_{RGB} parameter, ΔE_{RGB} was calculated according to the following equation [37,45]:

$$\Delta E_{RGB} = \sqrt{(R - R_0)^2 + (G - G_0)^2 + (B - B_0)^2}$$

where: R_0 G_0 and B_0 are the colours specified by the RGB colour space model of the control sample, and components R, G and B of the equation shown below correspond with the colour of solution/layer submerged in solution containing metal cations.

3. Results and discussion

3.1. Macrocycle synthesis and characterisation

Macrocycles bearing two azo groups and heterocyclic unit are relatively easily to prepare in diazocoupling reactions of the respective bisdiazonium salts with heterocyclic compounds (pyrrole, imidazole, methylimidazoles) carried out under high dilution conditions [37,45,47,49,50,57].

Continuing the saga of macrocyclic imidazole azoderivatives [37,45,49,50], here we present the synthesis (Scheme 1) of a new macrocycle, **5C2MeIm**, which to our best knowledge, has been obtained for the first time. **5C2MeIm** was obtained with 19% yield (for synthetic details, see Experimental). The yield of macrocyclisation was compared with the yield of oligoether analogue, macrocycle **3O2MeIm** (Scheme 1), obtained by us earlier [50]. The yield of macrocyclisation for 17-membered ring **3O2MeIm** was higher, 25%. These results are in agreement with those previously obtained for series of hydrocarbon and oligoether residue-linked macrocycles bearing imidazole or 4-methylimidazole heterocycle unit (Fig. 1).

The yield of macrocyclisation of imidazole-derived chromogenic compounds falls in the range of 19-55%. By comparison of the series it might be concluded that macrocyclisation yield is dependent on several factors. One of them is macrocycle ring size—the smaller the macroring, the lower the yield. It is well observed by comparison of macrocyclisation yields both for oligoether and hydrocarbon linked macrocycles (Fig. 1). It might be explained by the greater ring strain due to unfavourable bond angles and steric interactions in smaller rings. This strain makes the cyclisation process more challenging, lowering the yield. Larger macrorings have greater flexibility, allowing the reactive sites to align more favourably for cyclisation. Moreover, for hydrocarbon-linked compounds, higher yields were obtained for macrocycles with 4-methylimidazole than for these with unsubstituted imidazole unit [37]. For oligoether analogues, higher macrocyclisation yields were found for imidazole-than for 4-methylimidazole-bearing derivatives. The lowest yields were observed for 2-methylimidazole--bearing oligoether-linked azocrowns. The last can be easily explained by the fact that the most reactive position in diazocoupling reaction (2-position) in imidazole ring is occupied [58].

Having in mind the experiments carried out by Biernat and coworkers [59,60], where the influence of the cyclodextrin (CD) presence on diazocoupling reaction of bis-diazonium salts with heterocyclic compounds was investigated, in the pilot experimentwe re-synthetised 17-membered macrocycle **5C2MeIm** in the presence of cyclodextrins as molecular reactors (details in Experimental). As it was reported [60], the effect of the presence of cyclodextrins on the yield of macrocyclisation for **3O2MeIm** was more than significant. It was found that this compound can be obtained with 89% yield when diazocoupling was carried out in the presence of γ-CD (plain reaction 25%). In the case of the **5C2MeIm,** such spectacular effect was not observed. Less than

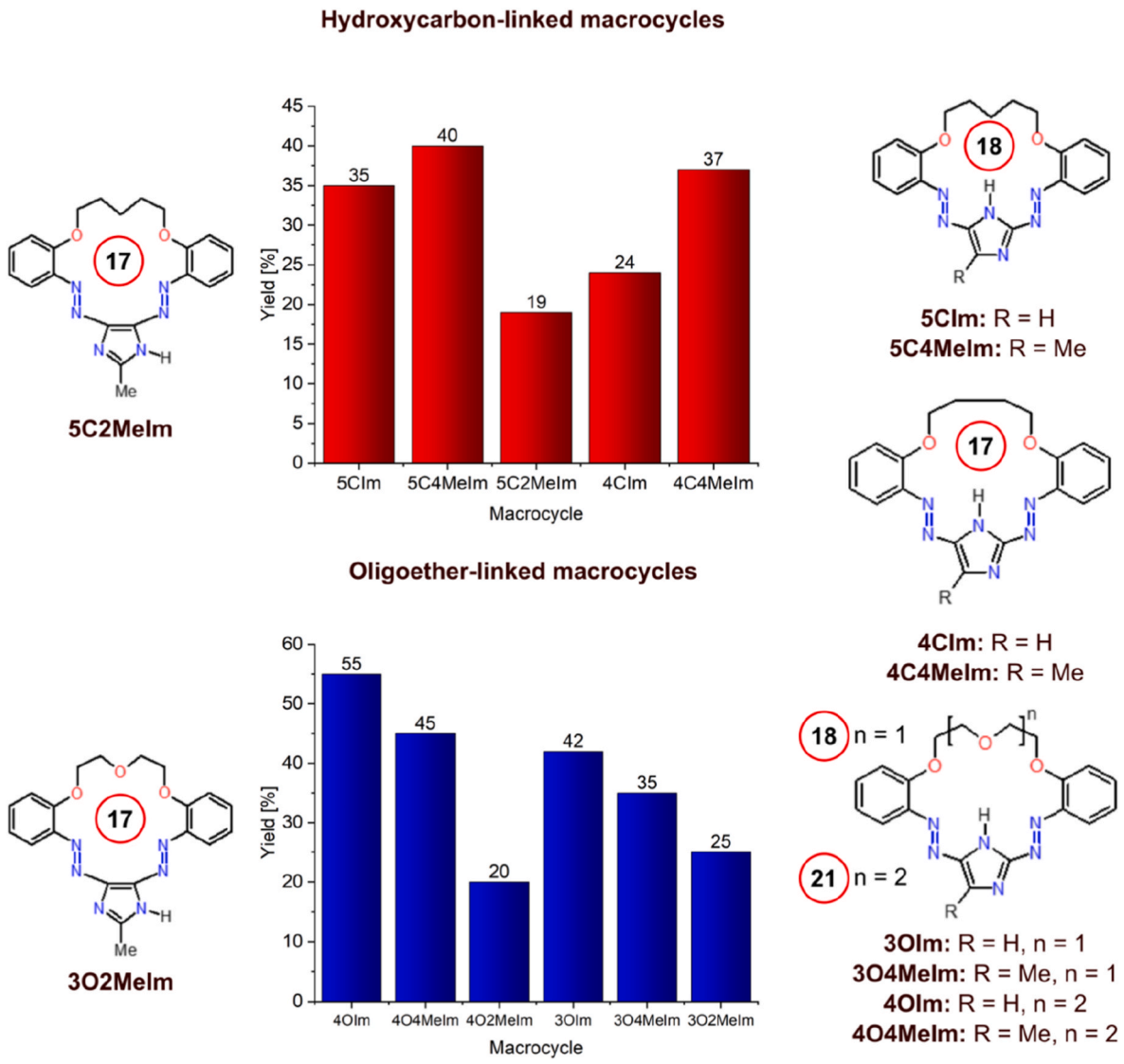

Fig. 1. The comparison of the macrocyclisation yield—synthesis of imidazole series of azomacrocycles [37,45,49,50].

moderate increase of yield was found: 21, 24, 22% in the presence of α-, β- and γ-CD, respectively. In plain reaction the yield of macrocyclisation for **5C2MeIm** was 19%.

CDs are known to form inclusion complexes with lipophilic substrates, which make them useful, among others, in food and drug industries [61]. It was found that there is a positive correlation between drug (namely profens) lipophilicity and the measured binding constant of complexes with CDs [62]. However, this hardly explains the low yield of **5C2MeIm**. When assuming the possible interactions between CDs and intermediate, it can be noted that when less lipophilic substrate, which bears an oligoether linker, is analysed, some of its interactions with CD's hydroxyl groups (namely hydrogen bonds) can be considered. Macrocycle with hydrocarbon linker has one hydrogen bond acceptor less than its oligoether analogue, thus the stabilisation of the intermediate of diazocoupling via hydrogen bonding can be less effective. Inclusion complex stabilisation involving hydrogen bonding between guest and the 3C–OH group of cyclodextrin has been reported in the literature [63]. The comparison of some physicochemical properties of **3O2MeIm** and **5C2MeIm**, calculated with SwissADME software [64], is listed in Table S2. Plausible model of interaction of intermediate with CD,

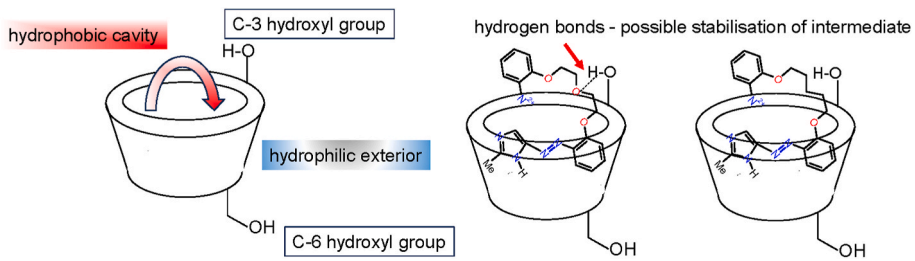

Fig. 2. Schematic illustration of a possible host–guest preorganisation scenario during diazocoupling in the presence of cyclodextrin. The extent of inclusion may differ depending on substrate structure.

leading to **3O2MeIm** and **5C2MeIm**, is proposed in Fig. 2. The detailed investigation of the effect of molecular reactors, CDs, on the macrocyclisation of the series of azocrowns with imidazole residue is ongoing in our lab. Results will be compared with data published by Biernat et al. [60].

To gain additional insight into the role of cyclodextrins as molecular reactors in these systems, we performed 2D NMR studies of the interactions between the ligands and β-cyclodextrin in aqueous solution. In these experiments β-cyclodextrin was chosen as a model host, because it is commercially most accessible and widely used in supramolecular studies; here it served as a representative cyclodextrin to qualitatively probe the inclusion behaviour of both **3O2MeIm** and **5C2MeIm** in water. In D_2O **3O2MeIm**, which is poorly soluble in water, became soluble upon addition of an equimolar amount of β-cyclodextrin, indicating host–guest interaction. DOSY spectra revealed identical diffusion coefficients for **3O2MeIm** and β-cyclodextrin, consistent with the formation of a relatively stable inclusion complex. ROESY experiments showed intermolecular cross-peaks between aromatic protons of **3O2MeIm** and inner cavity protons of β-cyclodextrin (H3 and H5/H6, Fig. 3), confirming spatial proximity and inclusion-type binding.

In contrast, in a competitive D_2O/DMSO-d_6 (1:1) mixture, different diffusion coefficients were observed and no intermolecular ROESY cross-peaks were detected, indicating disruption of the complex by strong solvation.

Under analogous conditions, **5C2MeIm** did not exhibit NMR evidence of inclusion-type interaction with β-cyclodextrin.

These observations provide direct experimental support for differential host–guest behaviour of the two macrocycles and are consistent with the pronounced cyclodextrin-induced yield enhancement observed for 3O2MeIm and the minimal effect found for **5C2MeIm**. Representative DOSY and ROESY spectra are shown in Supplementary Information (Fig. S5a–S5f). Although direct stabilisation of the diazocoupling intermediate has not been experimentally demonstrated, the data support a qualitative preorganisation or confinement effect. These observations provide indirect, but consistent, support for the conclusion that β-cyclodextrin can act as an efficient molecular reactor for **3O2MeIm** by forming an inclusion complex in water, whereas such an effect is absent for **5C2MeIm**.

The values of lipophilicity for **3O2MeIm** and **5C2MeIm**, determined as $logP_{TLC}$, in two chromatographic systems, are presented in Fig. 4 and compiled in Table S3. According to previously observed trend [37], macrocycles linked with oligoether are less lipophilic than their hydrocarbon analogues. In the case of 2-methylimidazole-containing **5C2MeIm**, however, the deviation from this relationship is well seen when the mixture methanol:water (9:1, v/v) as mobile phase was used. Surprisingly, the value of $logP_{TLC}$ determined in this system is the lowest among all investigated macrocyclic azoderivatives of imidazoles. The reason for those disparities might be related to the position of the hydrogen-bearing nitrogen atom of imidazole ring. In previously investigated macrocyclic compounds with 4-methylimidazole, the hydrogen atom was directed towards the molecular cavity, which could possibly lead to the formation of intramolecular hydrogen bonds. In 2-methylimidazole the possibility of formation of analogous intramolecular hydrogen bond seems to be limited. Studies of molecular packing of series of imidazoles proved that molecules are linked by single N–H···N hydrogen bonds to the two neighbours, forming zigzag chains [63]. Such interactions are possible in case of studied here macrocyclic derivatives of 2-methylimidazole and less probable for macrocyclic derivatives of 4-methylimidazole, where N–H residue is set in the macrocyclic cavity. Thus, it can be concluded that the lower, unexpected lipophilicity of **5C2MeIm** can be the effect of the formation of the intermolecular hydrogen bond systems, which decrease the lipophilicity of the hydrocarbon linked macrocycle. The presence of strong hydrogen bonds is well seen in solid state in FTIR spectra (cf. Fig. S1d). The spectrum is characteristic, with a broad region between 3500 and 2500 cm^{-1}, which is similar to the spectral pattern of 2-methylimidazole, as studied by Hachuła [63]. In FTIR spectra of 4-methylimidazole--bearing macrocycles such spectral pattern is not observed [37]. Additionally, stronger hydrogen bonds were found in solution for 2-methylimidazole-bearing macrocycles. In ^1H NMR spectra registered in DMSO-d_6 the signal of N–H proton is observed at ~13 ppm (Fig. S1a for **5C2MeIm** and Fig. S2 for **3O2MeIm**), whereas for 4-metylimidazole derivatives at ~ 10.3 ppm (Fig. S3 for **5C4MeIm** and Fig. S4 for **3O4MeIm**).

As it is mentioned above, we used free online prediction tool SwissADME [64] for the characterisation of **3O2MeIm**, **3O4MeIm**, **5C2MeIm** and **5C4MeIm** (cf. Table S2). Additionally, we calculated HLB (Hydrophile-Lipophile Balance) for above macrocycles using McGowan [65] and Griffin [66] approach (Table 1). For calculation details see Supplementary Materials.

When comparing calculated values for isomeric macrocycles and experimental lipophilicity values ($logP_{TLC}$) obtained using RP-TLC

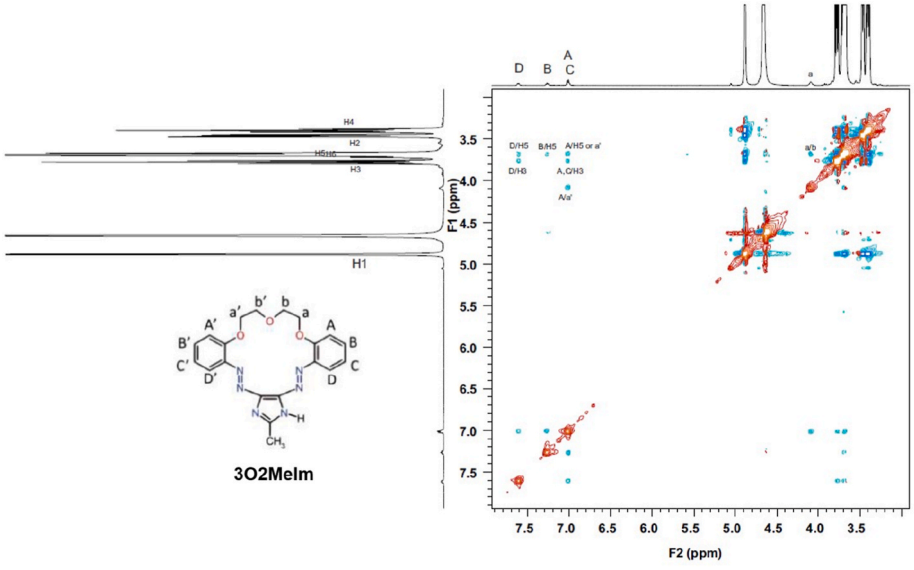

Fig. 3. ROESY spectrum of an equimolar mixture of **3O2MeIm** and β-cyclodextrin in D_2O. Intermolecular cross-peaks between aromatic protons (A–D) of the ligand and inner cavity protons (H3 and H5/H6) of β-CD confirm spatial proximity consistent with host–guest interaction.

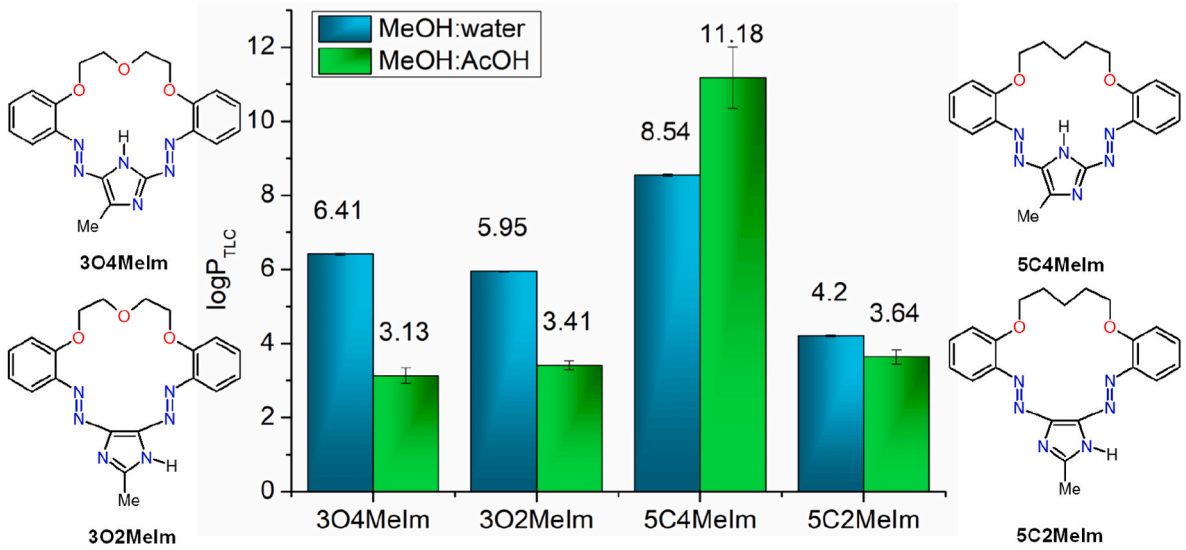

Fig. 4. The comparison of the lipophilicity (logP) of a series of methylimidazole macrocycles determined by RP-18 TLC method using various mobile phases (this work and [37] for 4-methylimidazole derivatives) methanol:water (9:1) and methanol:acetic acid (9:1).

Table 1
Comparison of HLB and $V_x$valuesforinvestigated azomacrocyclic derivatives of isomeric methylimidazoles.

Formula	Macrocycle	HLB McGowan	HLB Griffin	Vx [cm^3/mol]	Number of H-bond acceptors	Number of H-bond donors
$C_{20}H_{20}N_6O_3$	**3O2MeIm** **3O4MeIm**	5.29	8.51	290.27	8	1
$C_{21}H_{22}N_6O_2$	**5C2MeIm** **5C4MeIm**	5.26	7.42	298.49	7	

method in methanol:water (9:1) system it is well seen that other factors, which are not included in used mathematical models, must affect the lipophilicity. The unexpectedly lower lipophilicity of the **5C2MeIm** isomer compared to **5C4MeIm** is most likely due to the mentioned above, accessibility of the N–H imidazole unit as a hydrogen bond donor. In **5C4MeIm** the N–H moiety is located inside the molecular cavity which makes it less accessible to hydrogen bonding solvent molecules (water) than in the case of **5C2MeIm**. The effect of hydrogen bond on the values of $logP_{TLC}$ determined by RP-TLC method was confirmed by the change of the mobile phase, where acetic acid was used instead of water. In this case the lipophilicity value for **5C2MeIm** is slightly higher than in water-containing system. The most lipophilic macrocycle under these conditions is still **5C4MeIm**.

Our case shows that lipophilicity values obtained by TLC method must be carefully considered, as the chromatographic conditions, along with the individual character and structure of the analytes, can affect these values. It is in agreement with remarks and comments included in exhaustive review articles [67,68]. This also highlights the shortcomings of computational models which may not be sensitive to structural differences of studied chemical compounds. Our results are to a large extent in agreement with the studies by other authors concerning the relationship between hydrogen-bonded systems and their lipophilicity [51,69].

3.2. Metal cation complexation studies

Previously we have reported the complexation properties of the series of azocrowns with imidazole/4-methylimidazole heterocycle unit [37,45,50]. It was shown that metal cation complexation properties (e.g. stability constant values of metal complexes, selectivity, colour change), both in solution and after immobilisation of chromoionophore in sensing layer is dependent on the macrocycle size and also influenced by the substitution of imidazole ring. It could be deducted that ionisable N–H residue directed inside the molecular cavity of the macrocycle is crucial for strongly coloured complexes. Ionisable chromoionophores are relatively widely described in older [70–73] and newer literature [46,48,74–76], and it is well known that ionization of the molecule might strongly affect its absorption spectrum and, in result, colour [77].

We decided to investigate metal cation complexation properties of 17-membered azocrowns: **3O2MeIm** and newly obtained **5C2MeIm**, and compare their properties with previously obtained and studied by us macrocyclic imidazole derivatives. **3O2MeIm** was synthesised earlier, but was not investigated as a chromoionophore in solution. This macrocycle, when used as an ionophore in ion-selective electrodes was lead (II)-selective; unfortunately it readily leaked to the aqueous solution in the presence of Pb(II) [50]. For previously investigated imidazole derivatives, well pronounced colour change was observed in the presence of lead(II) and bismuth(III), both in solution and after immobilisation in polymer matrix [45]. It was found that smaller ring macrocycles (18-membered) are better chromoionophores in optical sensing layers than their 21-membered analogues. In the current investigation of complexation properties, we consider the influence of the macrocycle size, the type of linker, and the substitution pattern of the imidazole heterocyclic residue, which governs the orientation of the ionisable N–H group either inward or outward relative to the macrocyclic cavity.

Thus the first experiments covered quantitative probes to estimate colour changes of solutions of **3O2MeIm** and **5C2MeIm** generated by the presence of metal salts. Results shown in Figs. 5 and 6 indicate that no spectacular colour change is observed in the presence of metal salts. For comparison: for oligoether macrocycles with imidazole or 4-methylimidazole colour changes in the presence of lead(II) and bismuth(III) salts were observed (from red to blue/violet) [37,45]. The most pronounced, but not spectacular, colour change for **3O2MeIm** and **5C2MeIm** was visible in the presence of copper(II), lead(II) and silver(I).

Colour change of solutions of **3O2MeIm** and **5C2MeIm** was analysed by Colour Digital Analysis (CDA) and expressed as ΔE_{RGB} parameter,

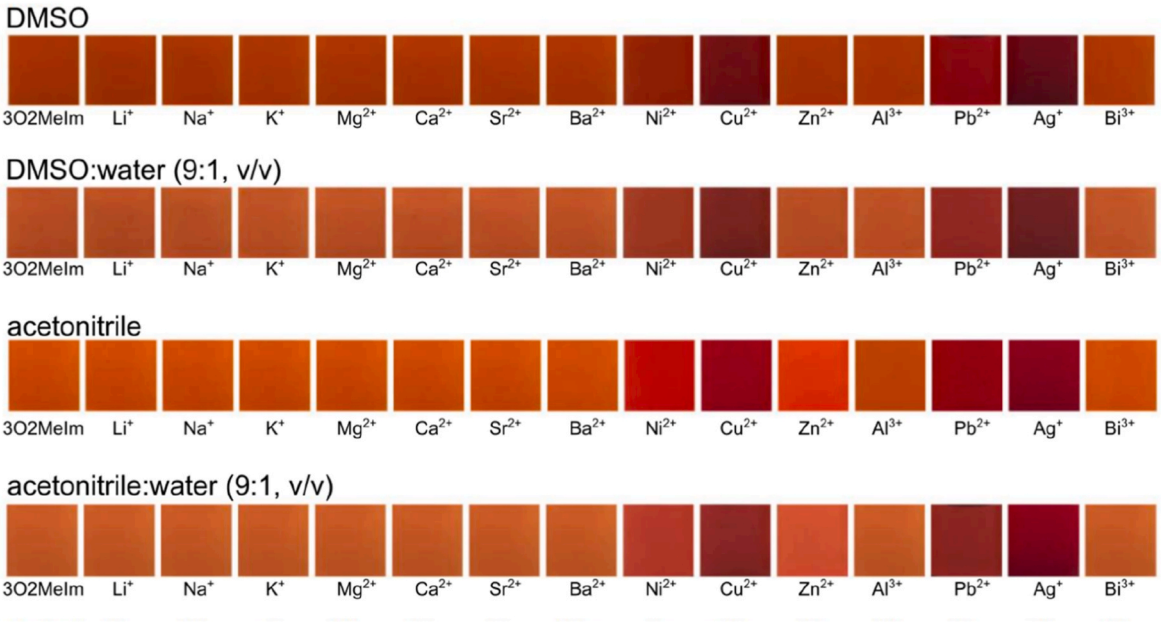

Fig. 5. Colour changes of the solutions of **3O2MeIm** in: DMSO ($3.94{\cdot}10^{-4}$ M), DMSO:water, 9:1,v/v ($3.75{\cdot}10^{-4}$ M), acetonitrile ($3.51{\cdot}10^{-4}$ M) and acetonitrile:water 9:1,v/v mixture ($3.51{\cdot}10^{-4}$ M) in the presence of metal salts (excess, added as solid). (For interpretation of the references to colour in this figure legend, the reader is referred to the Web version of this article.)

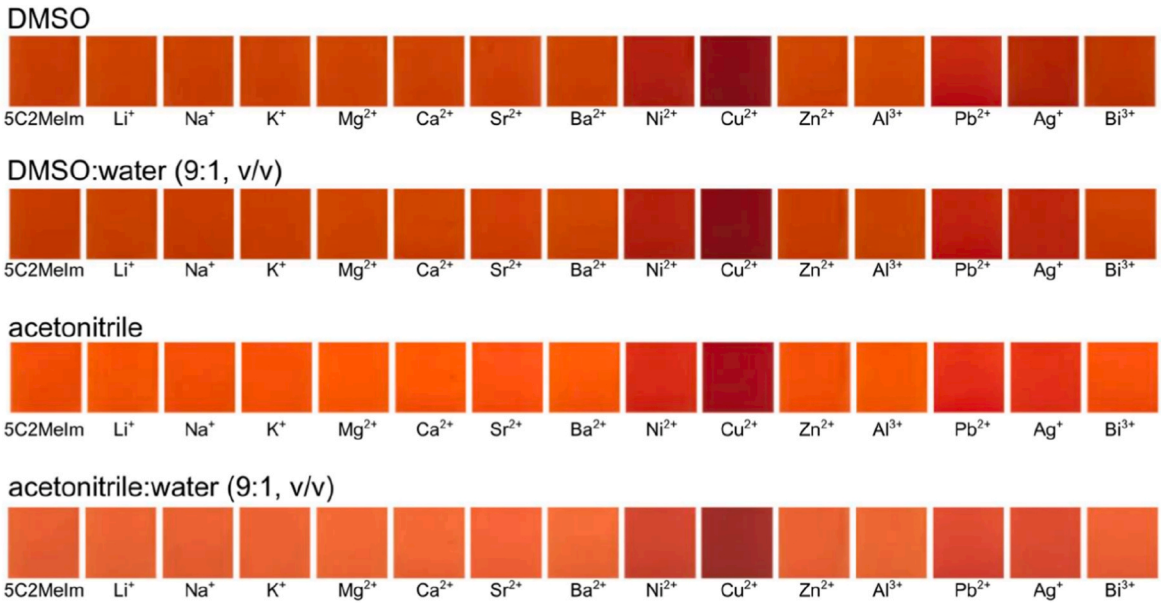

Fig. 6. Colour changes of the solutions of **5C2MeIm** in: DMSO ($3.34{\cdot}10^{-4}$ M), DMSO:water, 9:1,v/v ($3.18{\cdot}10^{-4}$ M), acetonitrile ($3.49{\cdot}10^{-4}$ M) and acetonitrile:water 9:1, v/v mixture ($3.32{\cdot}10^{-4}$ M) in the presence of metal salts (excess, added as solid). (For interpretation of the references to colour in this figure legend, the reader is referred to the Web version of this article.)

which is depicted in Fig. 7. For comparison, colour changes expressed as (R + G + B)/3 and I = 0.299R + 0.587G + 0.114B are presented in Supplementary Material in Figure S6 and Figure S7, respectively.

Results shown in Fig. 7 are in agreement with the visual observations of colour changes. However, the most significant information obtained from comparison of Fig. 7a and b is the selectivity of the generated colour change, which depends on both the type of the chromoionophore, as well as the metal cation used in quantitative experiment. Generated colour change is more selective in the case of **5C2MeIm**. Here, the highest value of the parameter ΔE_{RGB} is observed in all solvent systems for copper(II), whereas nickel(II), lead(II) and silver(I) might be considered as interfering metal cations. For **3O2MeIm**, comparing with **5C2MeIm** of the same macrocycle ring size, the change of the coordination atom number, namely oxygen in oligoether linkage, decreases selective colour change. It is in agreement with previously investigated analogues bearing imidazole or 4-methylimidazole heterocyclic residue [37].

From the comparison of the results of above mentioned simple experiments it is well seen that observed colour change upon metal cation interaction in solutionis not as spectacular as it was in thecase of the 18-membered unsubstituted imidazole derivatives and 4-methylimidazole analogues; the latter changed colour from orange/red to blue/violet in

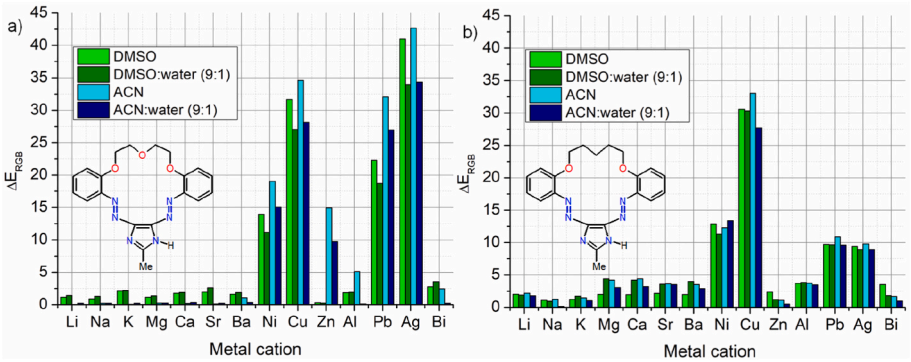

Fig. 7. Comparison of the colour change of solutions of a) **3O2MeIm** and b) **5C2MeIm** in the presence of the excess of metal salts, expressed as ΔE_{RGB} parameter. (For interpretation of the references to colour in this figure legend, the reader is referred to the Web version of this article.)

the presence of lead(II) and bismuth(III) salts [37,45].

The UV-Vis spectrophotometric method was used to describe the metal cation complexation properties of the **5C2MeIm** and **3O2MeIm** macrocycles. **5C2MeIm** and **3O2MeIm** were titrated with metal perchlorates in both acetonitrile:water (9:1, v/v) and DMSO:water (9:1, v/v) systems. However, in the DMSO:water (9:1, v/v) system, it was not possible to achieve equilibrium under the previously established spectrophotometric titration conditions, and therefore it was not possible to calculate reliable binding constant values. Time-dependent changes in absorbance were observed during titration and no stable spectral plateau was reached within the experimental time scale. This is consistent with the complex, highly non-ideal solvation processes described for mixtures of water and DMSO, which can complicate binding equilibrium measurements even at low DMSO volume fractions [78–80]. In particular, water–DMSO mixtures exhibit microheterogeneous organisation and preferential solvation effects, which may result in time-dependent redistribution of solvent shells around the interacting species. Therefore, the following section discusses only the results of metal cation complexation in an acetonitrile:water (9:1, v/v) system. The mixed acetonitrile-water solvent was chosen because of its potential applications in predominantly aqueous environments and to avoid the equilibrium problems encountered in DMSO:water [81,82].

The UV-Vis spectrum of **5C2MeIm** registered in acetonitrile:water mixture consists of three peaks: a sharp maximum at 301 nm ($\varepsilon 1.26{\cdot}10^4$), a broad band in 358-400 nm region, and a smaller, less pronounced peak at 466 nm ($\varepsilon 9.76{\cdot}10^3$) (Fig. 8). To estimate the nature of the complex formation (stoichiometry and stability constant of the complexes) metal cation salts were chosen, which displayed the most significant changes in quantitative tests. **5C2MeIm** was titrated with $Cu(ClO_4)_2$ in the acetonitrile:water (9:1, v/v) system. The changes in UV-Vis spectrum in this system (pictured in Fig. 8a) are well pronounced, as the hypochromic effect can be seen in both 301 nm and 379 nm peaks. The most noticeable change is observed within the maximum (466 nm): a bathochromic shift to 506 nm occurs, and the absorbance increases when more salt is introduced to the system. Confirmed by Job's method (Fig. S8a), it was concluded that **5C2MeIm** (under titration conditions) forms complexes with copper(II) of 3:2 (crown:metal) stoichiometry—possibly a triple-decker sandwich type (three macrocyclic ligands stacked around two metal centres). The calculated value of binding constant, given as logK, is 18.55 ± 0.58 in acetonitrile:water (9:1, v/v) system. In acetonitrile:water (9:1, v/v) system, which is depicted in Fig. 8b, the changes in the UV-Vis spectrum generated by titration with lead(II) perchlorate are not spectacular and require rather high concentration of lead(II) salt in the system. Nevertheless the response is visible throughout the entire spectrum. The peak observed at 301 nm gets bathochromically shifted to 313 nm. The broad maximum at 388-400 nm becomes more narrow, with a pronounced peak at 368 nm, and a hyperchromic effect within it can be noted. Peak at 466 nm is broader the more lead(II) perchlorateis present in the system, and a bathochromic shift to 477 nm is observed. The stoichiometry of the complex forming in acetonitrile is 2:1 (crown:Pb(II)), as confirmed by Job's method (Fig. S8b), with binding constant in acetonitrile:water (9:1, v/v) system logK 7.02 ± 0.22. That is in opposition to its previously reported analogue, **5C4MeIm**, which in acetonitrile and its mixture with water forms triple-decker sandwich type complexes (3:2 stoichiometry) [37]. There is a possibility that the disparity between the complexation of lead (II) by **5C2MeIm** and **5C4MeIm** stems from the position of the NH group in the methylimidazole part of the compound.

It can be concluded that contrary to previously investigated compounds [37], **5C2MeIm** displays affinity not only to the lead(II) ions, but also to copper(II) ions in acetonitrile:water (9:1, v/v) system.

The UV-Vis spectrum of **3O2MeIm** is similar to the spectrum of **5C2MeIm** and consists of three peaks: at 300 nm ($\varepsilon 1.81{\cdot}10^4$), at 463 nm ($\varepsilon 1.33{\cdot}10^4$) and a broad band between 348 and 405 nm. Upon titration with copper(II) perchlorate in the acetonitrile:water (9:1, v/v) system, depicted in Fig. 9a, a hypochromic effect can be observed within the

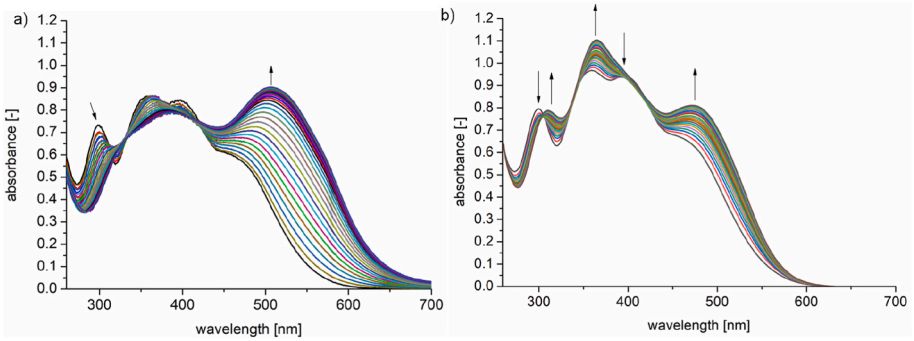

Fig. 8. Changes in UV-Vis spectrum of: a) **5C2MeIm** ($c = 3.94{\cdot}10^{-5}$ M) upon titration with copper(II) perchlorate ($c = 0\text{-}3.05{\cdot}10^{-4}$ M); b) **5C2MeIm** ($c = 4.21{\cdot}10^{-5}$ M) upon titration with lead(II) perchlorate ($c = 0\text{-}1.43{\cdot}10^{-3}$ M) in acetonitrile:water (9:1, v/v) system.

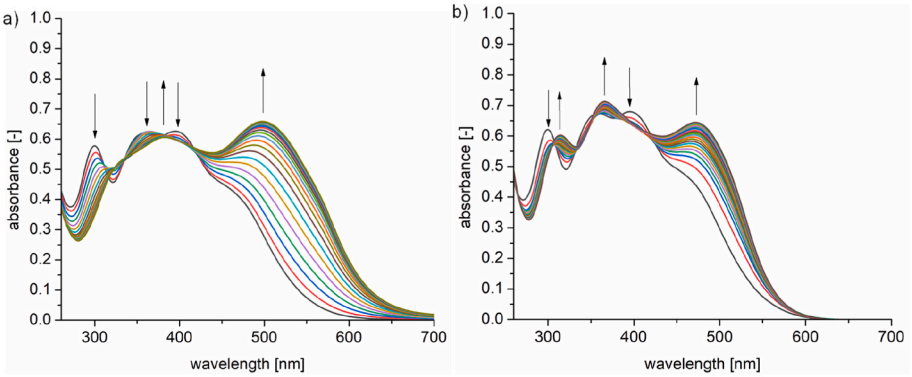

Fig. 9. Changes in UV-Vis spectrum of: a) **3O2MeIm** ($c = 3.32 \cdot 10^{-5}$ M) upon titration with copper(II) perchlorate ($c = 0\text{-}5.72 \cdot 10^{-5}$ M); b) **3O2MeIm** ($c = 3.42 \cdot 10^{-5}$ M) upon titration with lead(II) perchlorate ($c = 0\text{-}1.42 \cdot 10^{-3}$ M) in acetonitrile:water system (9:1, v/v).

peak at 300 nm. The broad maximum at 348-405 nm gains a more pronounced peak at 385 nm. The biggest difference can be seen within the peak at 463 nm—it is affected by the hyperchromic effect, as well as a bathochromic shift to 498 nm. These changes overall correspond to the optical effect—a orange-yellow solution becomes red. In the same solvent system, **3O2MeIm** forms complexes also with lead(II) cations (Fig. 9b). Similarly to the complexes of **5C2MeIm** with those cations, the changes in UV-Vis spectrum are only visible upon titrating with a relatively high-concentration solution of salt. The peak at 300 nm undergoes a bathochromic shift and becomes less intense. The broad maximum at 348-405 nm becomes more pronounced, with the highest value of absorbance registered for 369 nm. The biggest change is observed for the peak at 463 nm, which is affected by both hyperchromic effect and bathochromic shift to 472 nm.

To estimate the stoichiometry of complexes formed under titration conditions, Job's plots were analysed. In both cases, namely copper(II) and lead(II) titrations, it is well seen that the maximum of the Job's plot is shifted depending on the chosen wavelength. It was confirmed by Job's method (Fig. S8c) that **3O2MeIm** forms in acetonitrile two types of complexes with copper(II) cations: a 2:1 sandwich (one metal centre bound between two macrocyclic ligands) and a 3:2 triple-decker type sandwich. Calculated for the acetonitrile:water (9:1, v/v) system, the OPIUM program [52] returns more accurate binding constant for 2:1 complex, which is equal to 8.88 ± 0.27. Similarly to the copper(II) complex, complexation of lead(II) by **3O2MeIm** in acetonitrile:water system can occur in two stoichiometries: 2:1 and 3:2, as confirmed by Job's method (Fig. S8d). Binding constant in acetonitrile:water (9:1, v/v) system was calculated by OPIUM program [52] for the 2:1 complex, returning the value of 7.43 ± 0.31. The values of stability constants of complexes of **3O2MeIm** and **5C2MeIm** are shown in Table S4.

Similarly to **5C2MeIm**, **3O2MeIm** displays affinity for lead(II) and copper(II) ions; the latter was not observed for the previously investigated analogue, **3O4MeIm** [37]. In fact, **3O2MeIm** displays higher affinity to copper(II) ions than lead(II). For previously investigated macrocycles with imidazole or 4-methylimidazole spectral changes were more pronounced upon lead-crown interactions. In the presence of copper(II) spectral changes were negligible and determination of the stability constants of formed under titration conditions was not possible. The most significant difference, comparing previously investigated imidazole macrocycles, found during conducted investigations is that no spectral and colour changes were observed for **5C2MeIm** and **3O2MeIm** in the presence of bismuth(III). In general, less pronounced colour changes were observed visually upon formation of metal cation complexes by 2-methylimidazole-bearing bisazocrowns, indicated by a rather small bathochromic shift of the complex absorption band.

To evaluate the influence of counter-anions on metal–ligand complexation equilibria and spectral response, supplementary UV -Vis titration experiments were carried out with copper(II) chloride, copper (II) nitrate, and lead(II) nitrate in acetonitrile:water (9:1, v/v). The results were compared with those obtained for the corresponding perchlorate systems.

The spectral changes observed upon addition of Cu(II) and Pb(II) salts remain qualitatively similar irrespective of the counter-anion employed. As shown in Figs. S9 and S10 (Supplementary Material), the general trend of the UV -Vis spectra follows the same pattern for perchlorate, nitrate and chloride salts. The most noticeable, yet not spectacular, difference is observed for copper(II) chloride, where the absorption maximum at ca. 385 nm for **3O2MeIm** and 379 nm for **5C2MeIm** is slightly red-shifted and exhibits lower intensity compared to the nitrate and perchlorate systems (Figs. S9a and S10a). Apart from this moderate effect, no substantial changes in band position or overall spectral pattern are observed.

The comparison of stability constants further supports the limited role of the counter-anion. As presented in Fig. 10, the logK values for Cu (II) complexes remain within the same order of magnitude for all investigated salts. For **3O2MeIm**, the 2:1 (L:M) complexes display logK values of 8.88 (perchlorate), 8.63 (nitrate) and 8.41 (chloride), while for **5C2MeIm** the corresponding 3:2 species exhibit logK values of 18.55 ± 0.58, 18.43 ± 0.08 and 18.84 ± 0.02, respectively. These differences are small and do not indicate a change in the dominant complexation mode.

For Pb(II), the stability constants determined for perchlorate and nitrate salts are also comparable. As shown in Fig. 11, **3O2MeIm** forms 2:1 (L:M) complexes with logK values of 7.43 ± 0.31 for lead(II) perchlorate and 6.95 ± 0.04 for lead(II) nitrate.

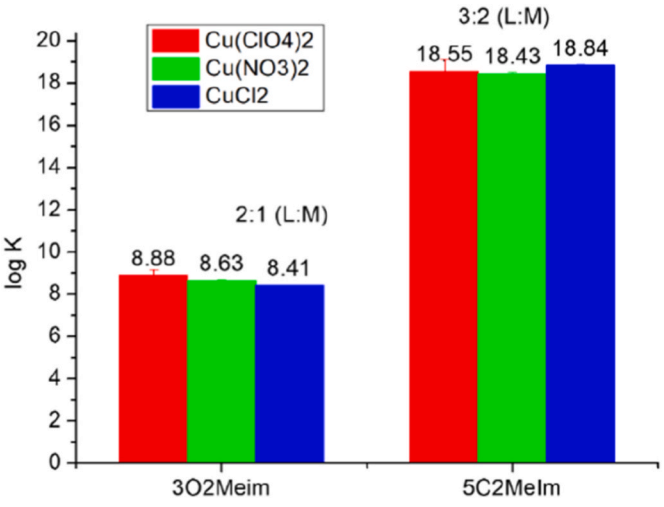

Fig. 10. Comparison of stability constants (logK) for Cu(II) complexes of **3O2MeIm** and **5C2MeIm** with different counter-anions (perchlorate, nitrate and chloride) in acetonitrile:water (9:1, v/v).

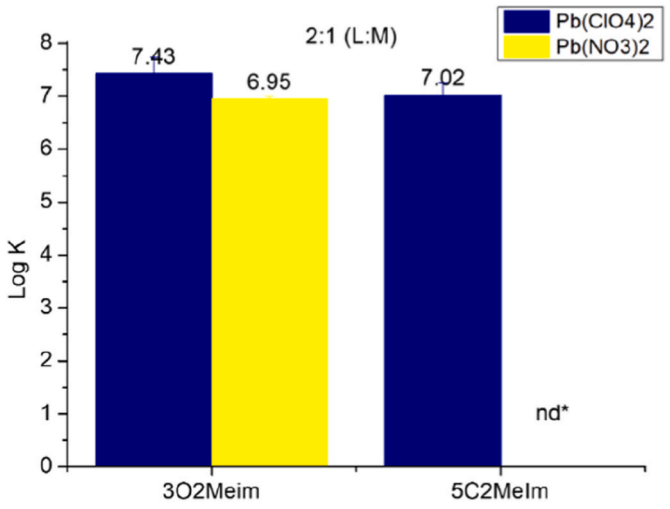

Fig. 11. Stability constants (logK) of Pb(II) complexes of **3O2MeIm** and **5C2MeIm** determined for perchlorate and nitrate salts in acetonitrile:water (9:1, v/v). The value for the lead(II) nitrate-**5C2MeIm** system could not be reliably determined (nd).

In the case of **5C2MeIm**, the 2:1 complex with lead(II) perchlorate is characterised by logK = 7.02 ± 0.22. For the lead(II) nitrate-**5C2MeIm** system, only minor spectral variations were observed even at relatively high metal salt concentrations (Fig. S10c), resulting in insufficient curvature of the titration profiles for reliable logK estimation. Consequently, no statistically reliable stability constant could be extracted and this system is reported as nd (Fig. 11).

Overall, both the spectroscopic data (Figs. S9 and S10) and the derived stability constants (Figs. 10 and 11) indicate that, under the applied experimental conditions, the counter-anion has only a secondary influence on the complexation behaviour. The binding strength and dominant stoichiometry are primarily governed by the nature of the metal ion and the structural features of the ligand.

To evaluate the influence of common interfering metal ions on complex formation, competition experiments were performed for both macrocyclic ligands, **3O2MeIm** and **5C2MeIm**, in acetonitrile:water (9:1, v/v). Preformed complexes with Pb(II) or Cu(II) were titrated with equimolar Zn(II) and Ni(II) (and with Cu(II) in the case of Pb(II) complexes), and the spectral changes were monitored by UV -Vis spectroscopy.

For the Cu(II) complexes of both macrocycles, titration with equimolar amounts of Zn(II) or Ni(II) salts produced only very minor changes in the UV-Vis spectra (Figs. 12 and 13).

The band shapes and absorption maxima remained essentially unchanged, and the small variations in absorbance are within the experimental error. These observations indicate that Zn(II) and Ni(II) act as weak interferents for Cu(II) binding by both **3O2MeIm** and **5C2MeIm**.

In contrast, the Pb(II) complexes of both macrocycles are significantly more sensitive to the presence of other metal ions. When lead(II) perchlorate complexes were titrated with equimolar copper(II) perchlorate pronounced bathochromic shift of the diagnostic bands were observed in spectra of both ligands (Fig. 14): for **3O2MeIm** the absorptions at ca. 369 nm and 472 nm shifted to ca. 385 nm and 498 nm, whereas for **5C2MeIm** the bands at ca. 368 nm and 477 nm shifted to ca. 379 nm and 506 nm. These changes clearly demonstrate efficient competition of Cu(II) with Pb(II) for coordination to both macrocycles.

Titrations with Ni(II) led to smaller but still noticeable spectral changes (Fig. 15), while Zn(II) mainly increased the absorbance at the existing maxima without significantly affecting the band shapes (Fig. 16).

The qualitative trends observed in Figs. 12–16 are quantitatively reflected in the Relative Response Percentage (RR%) values (Fig. 17), calculated at the most diagnostic wavelengths for both ligands.

For the Cu(II) complexes of **3O2MeIm** and **5C2MeIm**, RR% values in the presence of equimolar Zn(II) and Ni(II) remain below 5%, confirming their weak interfering character. In contrast, for the Pb(II) complexes of both macrocycles, Cu(II), Ni(II) and Zn(II) produce significantly higher RR% values, with Cu(II) being the strongest interferent, followed by Ni(II) and then Zn(II). Importantly, the magnitude of the interference depends on the monitored wavelength, as different bands respond with different RR% values. This indicates that the apparent impact of competing metal ions can be moderated by the choice of analytical wavelength, providing an additional handle to optimize the analytical response. Full titration spectra for all systems, as well as complete RR% profiles at all relevant wavelengths, are provided in the Supplementary Material (Figs. S11–S30).

Overall, these competition experiments show that both macrocycles exhibit very similar interference patterns: they bind Cu(II) robustly in the presence of Zn(II) and Ni(II), whereas their Pb(II) complexes are more susceptible to displacement or perturbation by these competing metal ions, with a wavelength-dependent spectral response.

To evaluate the effect of acidic and basic environment on the optical response, we examined the colour and spectral response of **5C2MeIm** and **3O2MeIm** towards Cu(II) and Pb(II) in acetonitrile:aqueous nitric acid (1:1, v/v) and acetonitrile:TRIS (1:1, v/v) mixtures.

For Cu(II), comparing with Pb(II), acidic conditions were clearly more favourable: in acetonitrile:aqueous nitric acid (1:1, v/v) both ligands exhibited well-defined bathochromic shifts of the main π–π* bands and a pronounced increase of the visible band (≈460–480 nm) upon Cu(II) addition, consistent with efficient complex formation under acidic conditions (Fig. S31a and c). In contrast, in acetonitrile:TRIS (1:1, v/v), no significant spectral changes were observed upon Cu(II) addition (Fig. S31b and d), which can likely be attributed to the competitive

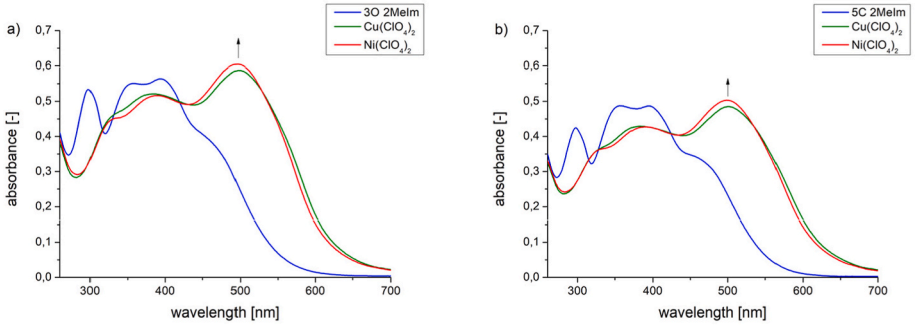

Fig. 12. Changes in UV-Vis spectrum of: a) **3O2MeIm** (c = $3.42{\cdot}10^{-5}$ M) with copper(II) perchlorate (c = $3.30{\cdot}10^{-5}$ M) upon titration with nickel(II) perchlorate (c = 0-$3.30{\cdot}10^{-5}$ M) in acetonitrile:water system (9:1, v/v), b) **5C2MeIm** (c = $4.21{\cdot}10^{-5}$ M) with lead(II) perchlorate (c = $5.11{\cdot}10^{-4}$ M) upon titration with nickel(II) perchlorate (c = 0-$5.11{\cdot}10^{-4}$ M) in acetonitrile:water system (9:1, v/v).

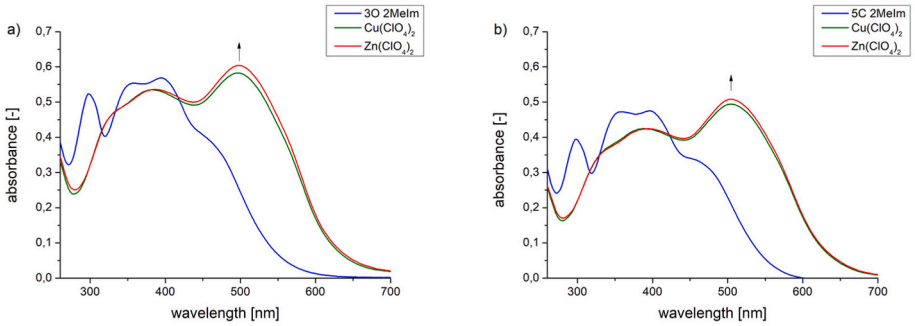

Fig. 13. Changes in UV-Vis spectrum of: a) **3O2MeIm** ($c = 3.42 \cdot 10^{-5}$ M) with copper(II) perchlorate ($c = 3.30 \cdot 10^{-5}$ M) upon titration with zinc(II) perchlorate($c = 0–3.30 \cdot 10^{-5}$ M) in acetonitrile:water system (9:1, v/v), b) **5C2MeIm** ($c = 3.32 \cdot 10^{-5}$ M) with copper(II) perchlorate ($c = 3.30 \cdot 10^{-5}$ M) upon titration with zinc(II) perchlorate ($c = 0–3.30 \cdot 10^{-5}$ M) in acetonitrile:water system (9:1, v/v).

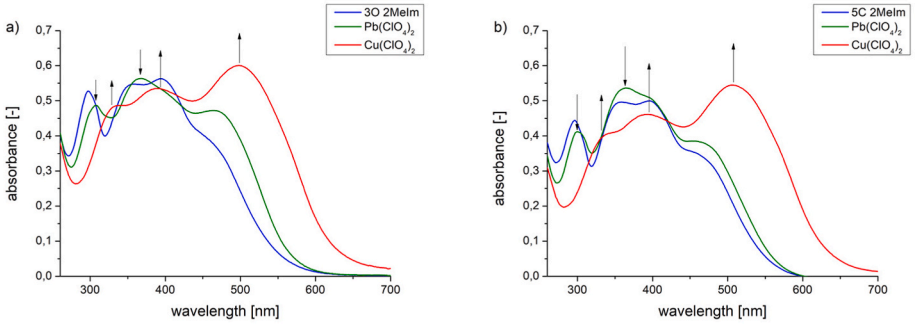

Fig. 14. Changes in UV-Vis spectrum of: a) **3O2MeIm** ($c = 3.42 \cdot 10^{-5}$ M) with lead perchlorate ($c = 5.11 \cdot 10^{-4}$ M) upon titration with copper perchlorate ($c = 0–5.11 \cdot 10^{-4}$ M) in acetonitrile:water system (9:1, v/v), b) **5C2MeIm** ($c = 4.21 \cdot 10^{-5}$ M) with lead perchlorate ($c = 5.11 \cdot 10^{-4}$ M) upon titration with copper perchlorate ($c = 0–5.11 \cdot 10^{-4}$ M) in acetonitrile:water system (9:1, v/v).

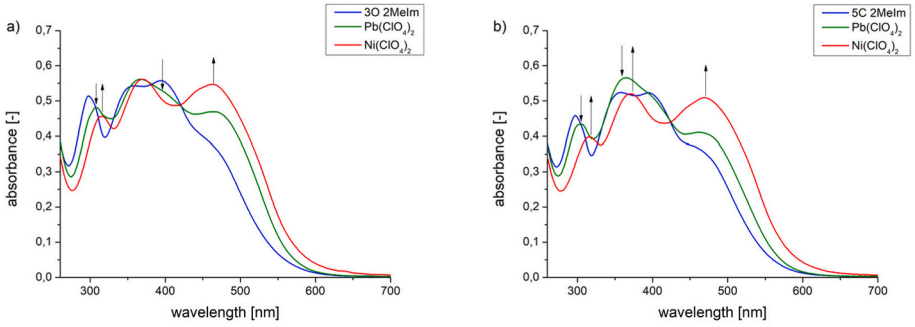

Fig. 15. Changes in UV-Vis spectrum of: a) **3O2MeIm** ($c = 3.42 \cdot 10^{-5}$ M) with lead perchlorate ($c = 5.11 \cdot 10^{-4}$ M) upon titration with nickel perchlorate ($c = 0–5.11 \cdot 10^{-4}$ M) in acetonitrile:water system (9:1, v/v), b) **5C2MeIm** ($c = 4.21 \cdot 10^{-5}$ M) with lead perchlorate ($c = 5.11 \cdot 10^{-4}$ M) upon titration with nickel perchlorate ($c = 0–5.11 \cdot 10^{-4}$ M) in acetonitrile:water system (9:1, v/v).

formation of Cu(II)–TRIS complexes, as reported in the literature [83].

For Pb(II), spectra recorded in acetonitrile:aqueous nitric acid (1:1, v/v) showed virtually no difference between the free ligands and Pb(II)-containing solutions (the traces overlap within experimental error, Fig. S32), suggesting that under strongly acidic conditions protonation of the imidazole unit and/or changes in Pb(II) speciation disfavor the formation of a distinct chromogenic Pb(II) complex. By contrast, in acetonitrile:water (9:1, v/v) system used for UV-Vis titrations, addition of Pb(II) salt induces clear bathochromic shifts and the growth of a new, more intense band in the 470–500 nm region for both ligands, which is absent in the spectra of the free chromoionophores in acetonitrile:water (9:1, v/v) and in acetonitrile:aqueous nitric acid (1:1, v/v).

A direct comparison of the UV-Vis spectra of **5C2MeIm** and **3O2MeIm** in acetonitrile-water (9:1, v/v) versus acetonitrile:aqueous nitric acid (1:1, v/v) thus confirms that the visible colour changes observed upon Pb(II) addition in acetonitrile:water system arise from metal–ligand complexation, whereas pH-induced spectral changes of the free ligand do not reproduce the spectral signature of the Pb(II) complex.

These observations support our choice of mildly acidic, non-buffered acetonitrile:water (9:1, v/v) as the working medium for quantitative binding studies: it avoids strong competition from buffer ligands and precipitation of Pb(II) hydroxide species, while maintaining conditions compatible with effective coordination and a reproducible chromogenic response.

A quantitative comparison with our previously described imidazole-based chromoionophores further explains the reduced selectivity of Bi (III) in the present system. Earlier 18- and 21-membered macrocycles formed highly stable 3:2 triple-decker complexes with Pb(II) in acetonitrile:water (9:1, v/v), with logK values of approximately 19-20 [37]. Closely related 18-membered derivatives exhibited comparable stability

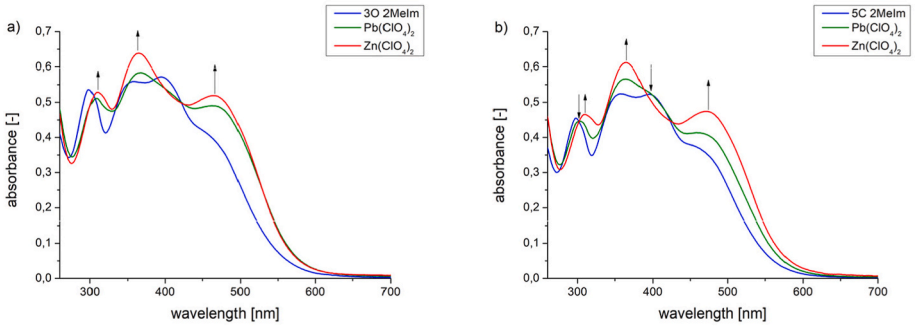

Fig. 16. Changes in UV-Vis spectrum of: a) **3O2MeIm** ($c = 3.42{\cdot}10^{-5}$ M) with lead(II) perchlorate ($c = 5.11{\cdot}10^{-4}$ M) upon titration with zinc(II) perchlorate ($c = 0–5.11{\cdot}10^{-4}$ M) in acetonitrile:water system (9:1, v/v), b) **5C2MeIm** ($c = 4.21{\cdot}10^{-5}$ M) with lead(II) perchlorate ($c = 5.11{\cdot}10^{-4}$ M) upon titration with zinc(II) perchlorate ($c = 0–5.11{\cdot}10^{-4}$ M) in acetonitrile:water system (9:1, v/v).

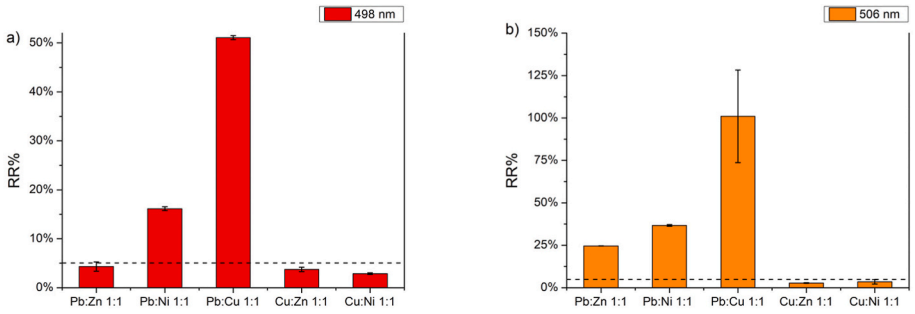

Fig. 17. Interferences of several metal perchlorates used at equimolar concentrations, expressed as RR%, to spectral response (ΔA) of a) **3O2MeIm** at 498 nm, b) **5C2MeIm** at 506 nm.

constants for Pb(II) and Bi(III) in DMSO:water (1:1, v/v), which translated into dual Bi(III)/Pb(II) selectivity in CTA-based optodes with detection limits in the range of 10^{-7} M for both cations [45].

In contrast, 17-membered bisazocrowns bearing 2-methylimidazole residue studied here bind Pb(II) in acetonitrile:water (9:1, v/v) only to a moderate extent (logK ≈ 7–8.9 for 2:1 or 3:2 species) and do not show any detectable complex formation with Bi(III) under similar conditions, i.e., no clear spectral or colour changes are observed; in practice, the LOD for Bi(III) is shifted outside the accessible concentration window, and it was not possible to develop a sensor layer selective for bismuth (III).

The loss of Bi(III) sensitivity can be connected with a combination of the several factors: (i) smaller cavity size (17-membered rings compared to 18/21-membered rings), (ii) altered orientation and limited availability of the ionisable N–H group in the 2-methylimidazole unit, which favors the formation of intermolecular rather than intramolecular hydrogen bonds. The same structural factors also provide a plausible rationale for the different Pb(II) stoichiometries observed for **5C2MeIm** and its regioisomer **5C4MeIm** [37,45]. While **5C4MeIm** readily forms 3:2 L_3Pb_2 "triple decker" complexes under comparable conditions, **5C2MeIm** predominantly affords 2:1 sandwich type L_2Pb species. Formation of higher order L_3M_2 assemblies requires cooperative engagement of donor atoms from three macrocyclic ligands around two Pb(II) centres; such species are expected to depend on a favourable spatial arrangement of imidazole donors and sufficient conformational flexibility of the macrocyclic framework. In **5C4MeIm**, the orientation of the imidazole N–H vector into the cavity, combined with a slightly larger and more accessible binding cavity, may facilitate this type of organisation. By contrast, the 2- methyl substitution in **5C2MeIm** enforces a different N–H direction and likely introduces additional steric constraints near the binding site, which may reduce the geometric adaptability required for formation of L_3Pb_2 species and shift the equilibrium towards simpler 2:1 complexes. In addition, in the present work complexation equilibrium is quantified in an acetonitrile:water (9:1, v/v) system, where both 2-methylimidazole bisazocrowns form only moderately stable Pb(II) complexes. Whereas in our earlier studies on larger macrocycles the more strongly hydrated DMSO:water (1:1, v/v) mixture favoured very stable 3:2 Bi(III)/Pb(II) species. In the specific case of **5C2MeIm** and **3O2MeIm**, the DMSO:water (1:1, v/v) system exhibits a complex equilibrium pattern, so that reliable stability constants could not be determined.

3.3. Copper(II) and lead(II) complexation in FTIR spectroscopy

Copper(II) and lead(II) complexation by **3O2MeIm** and **5C2MeIm** was investigated in solid state using FTIR (ATR) spectroscopy. Original spectra are shown is Supplementary Material (Figure S33 and Figure S34), along with the spectra of salts, namely copper(II) perchlorate and lead(II) nitrate (Figure S35 and Figure S36, respectively). FTIR band assignments of **3O2MeIm** and **5C2MeIm** and their shifts upon metal cation complexation are compiled in Table S5 and Table S6.

The FTIR spectra of the free macrocycles **3O2MeIm**, **5C2MeIM** and their complexes with Cu(II) and Pb(II) (Fig. 18) were analysed to identify shifts and changes in characteristic absorption bands upon complex formation.

The mentioned FTIR spectra reveal significant changes in the 1600–1300 cm^{-1}region. This spectral range includes stretching vibrations ν(C═N) and ν(C═C) (imidazole/benzene), bending vibrations δ(N–H), ν(N═N) vibrations of azo groups, and ν(C–N) [84–90]. In the FTIR spectra of both ligands and their complexes, the region 1600–1500 cm^{-1}, corresponding to ν(C═N), ν(C═C) (imidazole/benzene rings), and δ(N–H), shows only modest band shifts upon complexation. A distinction between Cu(II) and Pb(II) complexes can be observed by analysing the band at 1530 cm^{-1}. This band disappears (or becomes unresolved) in copper(II) complexes, whereas it remains clearly observable in the lead(II) complexes of both **3O2MeIm** and **5C2MeIm**. This may indicate a stronger perturbation of the π-conjugated system in

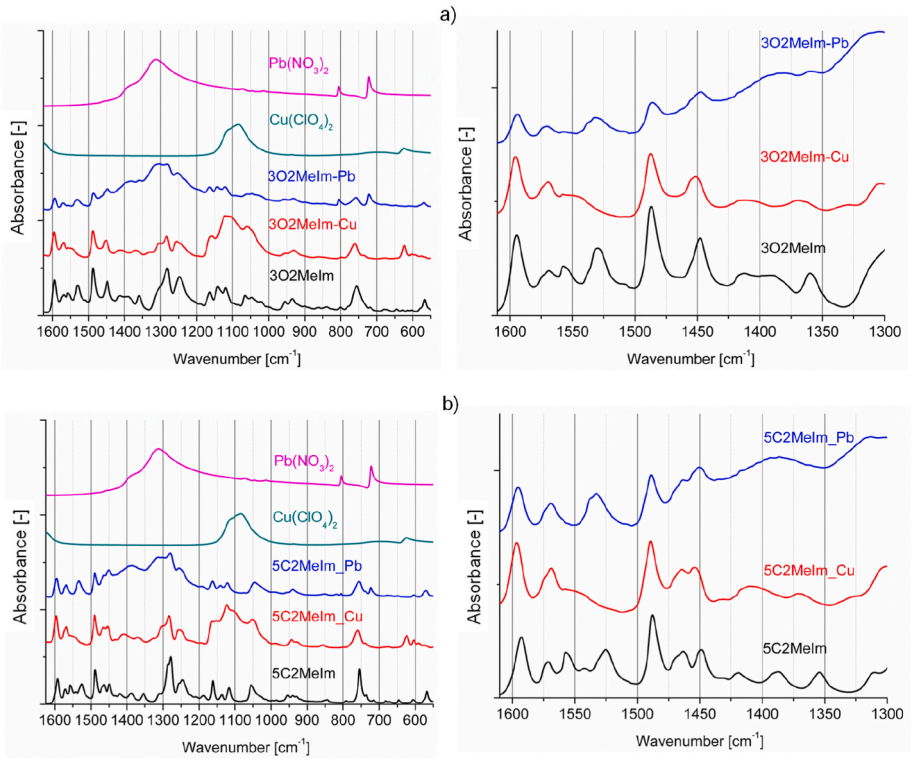

Fig. 18. The comparison of FTIR (ATR, normalised) partial spectra of: a) **3O2MeIm** b) **5C2MeIm** and their copper(II) and lead(II) complexes.

the case of copper(II) complexes. Moreover, the observed disappearance or merging of the ~1530 cm^{-1} band may suggest involvement of the nitrogen atom of the imidazole ring in metal coordination. Above findings are further supported by changes observed in the 1500–1300 cm^{-1} region, where contributions from ν(N═N), δ(C–H) (aromatic), and ν(C–N) vibrations can be assigned. For **3O2MeIm**, bands at 1448, 1412, and 1360 cm^{-1} undergo shifting and/or broadening: 1451, 1412 and 1369 in copper(II) complex. Similar changes are observed for copper(II) complex of **5C2MeIm**. In free macrocycle bands at 1463, 1449, 1419, 1387 and 1354 cm^{-1}, while in the complex they are located at 1464, 1454, 1410 and 1371 cm^{-1}. It should be noted here, that while copper (II) perchlorate does not interfere significantly in this spectral region, lead(II) nitrate shows a characteristic broad absorption band with a maximum at 1313 cm^{-1} (Fig. 18), which may partially overlap with the bands of complexes and limit interpretation. However, in the **3O2MeIm**–Pb complex, the peaks located at 1380 and in **5C2MeIm**–Pb at 1386 cm^{-1} (broader band) are clearly observable. It can suggest a different coordination mode for copper(II) and lead(II). Even if it is difficult to determine exactly which bands belong to which group in this region, the changes in the spectra (like shifts and broader bands) suggest that the azo group (–N═N–) takes part in forming the complexes, especially with lead(II) ions, most likely through coordination of a single nitrogen atom from one (or both) azo groups.

3.4. Lead(II) and copper(II) complexation in ^1H NMR spectroscopy

Lead(II) complexation was investigated in solution using ^1H NMR spectroscopy. Full, original spectra are shown in Supplementary

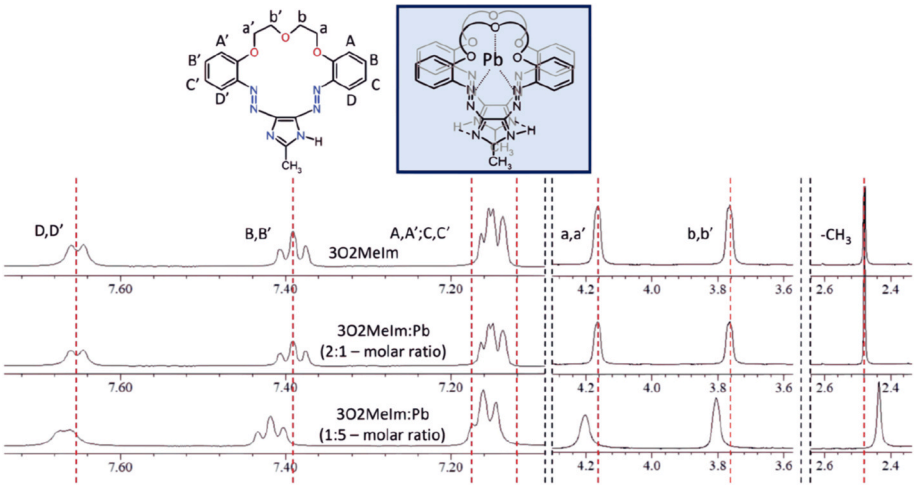

Fig. 19. ^1H NMR spectra of **3O2MeIm** and its lead(II) complexes (acetonitrile-d_3); in a blue frame plausible model of lead(II) binding. (For interpretation of the references to colour in this figure legend, the reader is referred to the Web version of this article.)

Material, Figure S37a-c and Figure S38a-c for **3O2MeIm** and **5C2MeIm**, respectively.

^{1}H NMR spectrum of **3O2MeIm** (acetonitrile-d_3) shows a single set of signals, which can be assigned to aromatic protons (Fig. 19), –CH_2- protons of oligoether moiety, and methyl group in 2-position of imidazole ring. Signal of N–H proton of imidazole ring is observed as a broad singlet. The positions of the proton signals of **3O2MeIm** and their shifts in spectra registered in the presence of lead(II) perchlorate are collected in Table 2. In the presence of five-fold molar excess of lead perchlorate, noticeable downfield shift of signals of aromatic protons D,D′ and B,B' (*ortho* and *para* position in relation to azo moiety, respectively) are seen. Moreover, signals of protons of oligoether linker are also downfielded, whereas signal of protons of methyl group is upfielded. One set of well-defined proton signals suggests one complex under measurement conditions. This can lead to the conclusion that lead(II) is coordinated through the oxygen atoms of oligoether linker and nitrogen atom(s) of azo moiety. Upfielded signal of methyl group of imidazole ring may suggest that this part of the molecule does not participate in complex formation in solution. In the complex, the imidazole N–H proton signal is slightly downfield shifted (+0.073), suggesting the change of the nature of intermolecular hydrogen bond comparing to the free crown.

Similar spectral pattern of protons observed in ^{1}H NMR spectrum of **5C2MeIm** (acetonitrile-d_3) shows a set of signals which can be assigned to aromatic protons (Fig. 20), methylene protons of Ar-*O*–CH_2– and methyl group in 2-position of imidazole ring. Signal of N–H proton of imidazole ring is observed as a broad singlet. The positions of the proton signals of **5C2MeIm** and their shift in spectra registered in the presence of lead(II) perchlorate are collected in Table 3. One set of well-defined proton signals suggests one complex under measurement conditions. As opposed to **3O2MeIm**, the spectral changes are observed in smaller molar amount of lead(II) perchlorate (2:1, crown:lead(II)), and are much more significant in the five-fold excess of lead(II). Noticeably the spectral pattern observed upon interaction with lead(II) perchlorate is different than in the case oligoether linked macrocycle. The largest spectral shift—downfield—is observed for signals of aromatic protons D, D′ and B,B' (*ortho* and *para* position in relation to azo moiety, respectively). Signals of methylene protons of ether grouping are upfielded, whereas signals of protons of methyl group of imidazole ring are downfielded. This can suggest a different lead(II) coordination mode in solution than for the oligoether analogue **3O2MeIm**.

The complexation of copper(II) in solution was additionally investigated using ^{1}H NMR for both ligands, **5C2MeIm** and **3O2MeIm**, in acetonitrile-d_3. The spectra recorded for samples prepared analogously to those used in FTIR experiments show clear changes compared to free macrocycles: all proton resonances are significantly broadened and partially merged, and the characteristic patterns of aromatic and aliphatic signals are largely lost. In particular, the imidazole N–H signal above 10 ppm shifts downfield (Δδ +1.78 ppm for **5C2MeIm**–Cu and +1.65 ppm for **3O2MeIm**–Cu). This behaviour, namely the significant broadening of lines characteristic of paramagnetic Cu(II) compounds, combined with a much greater downfield shift of N–H than in the corresponding Pb (II) complexes (Δδ +0.35 ppm for **5C2MeIm**–Pb and +0.07 ppm for **3O2MeIm**–Pb), can be explained by the coordination of Cu(II) in the vicinity of the imidazole/azo unit, but still does not allow for a detailed site-specific or stoichiometric analysis. In summary, these observations provide clear qualitative evidence for Cu(II) binding to both ligands in solution, while quantitative specifications and stoichiometry are obtained from UV-Vis titration and Job plots. The corresponding ^{1}H NMR spectra for free ligands and their Cu(II) adducts are provided in the Supplementary Material (Fig. S39).

^{1}H NMR spectra also confirm that similarly to previously described macrocyclic biazocrowns [37,45] bearing imidazole residue no *cis-trans* isomerisation is observed. It is important and advantageous when one considers the use of particular ligands as chelating agents as the number of species under equilibrium is limited.

Table 2
^{1}H NMR data for **3O2MeIm** and its lead(II) perchlorate complexes in acetonitrile-d_3;
$\Delta\delta = \delta_{complex} - \delta_{"free" crown}$; shifts in [ppm].

Proton assignment	3O2MeIm		
		crown:lead(II)	
	"free" crown	2:1	1:5
N–H	10.790, bs	10.863, bs (+0.073)	n.d.
-CH_3	2.478, s	2.477, s (−0.001)	2.432, s (−0.046)
a,a'	4.163, t, un	4.164, t, un (+0.001)	4.202, t, un (+0.039)
b,b'	3.764, t, un	3.764, t, un (n.c.)	3.805, t, un (+0.041)
A,A' + C,C'	7.127-7.172, m	7.127-7.172, m (n.c.)	7.133-7.181, m (+0.006,+0.009)
B,B′	7.391, t	7.391, t (n.c)	7.418, t (+0.027)
D,D′	7.651, d	7.652, d (+0.001)	7.668, d (+0.017)

n.d. – not detectable, n.c. – no changes, s – singlet,d – doublet, t – triplet, m – multiplet, b – broad, un – unresolved.

3.5. ESI-MS studies of Cu(II) and Pb(II) complexes

Low-resolution ESI-MS measurements were performed to qualitatively probe the speciation of Cu(II) and Pb(II) complexes formed by **5C2MeIm** and **3O2MeIm**. For both ligands, spectra of the free macrocycles show intense signals of the protonated species $[L + H]^+$ at *m/z* 391 (**5C2MeIm**) and 393 (**3O2MeIm**), accompanied by sodium adducts $[L + Na]^+$ at *m/z* 413 and 415, respectively, confirming the expected molecular masses.

In the presence of $Cu(ClO_4)_2$ additional Cu(II)-containing ions are observed in mass spectra for both macrocycles (Table S7–S8). For **5C2MeIm**, the spectrum shows a set of peaks at *m/z* 452–453 that can be assigned to a 1:1 Cu(II)–ligand adduct $[LCu]^+$/$[LCu\text{-}H]^+$, as well as higher-mass ions at *m/z* 842-845 and 1294-1296 that are compatible with $[2LCu]^+$ and $[3L2Cu]^+$, corresponding to 2:1 and 3:2 L:Cu stoichiometries, respectively. An analogous pattern is found for **3O2MeIm**: in addition to $[L + H]^+$ and $[L + Na]^+$, peaks at *m/z* 805-809, 846-850 and 1300-1301 can be tentatively assigned to $[2L + Na]^+$, $[2LCu]^+$ and $[3L2Cu]^+$, again indicating the presence of 2:1 and 3:2 L:Cu species. These LR-ESI-MS data confirm the formation of Cu(II)–ligand adducts and show the presence of several Cu-containing ions that are compatible with 1:1, 2:1 and 3:2 L:Cu compositions. This indicates that, in addition to the dominant complex detected under the UV-Vis titration conditions and modelled assuming a single prevailing stoichiometry, minor Cu(II)–ligand species of different L:Cu ratios are also present in solution. Given the low resolution of the LR-ESI-MS measurements and the pronounced clustering with Na^+, these assignments are considered as proposed rather than definitive and are used only as qualitative support for the speciation derived from UV-Vis data. Mass spectra of **5C2MeIm** and **3O2MeIm** showing their copper adducts are shown in Figures S40a-d and Figure S41a-c, respectively.

For samples containing $Pb(ClO_4)_2$, LR-ESI-MS spectra recorded for both **5C2MeIm** and **3O2MeIm** did not reveal any distinct ions that could be reliably attributed to discrete Pb(II)–ligand adducts. In both positive and negative ion modes, only signals corresponding to the free ligands ($[L + H]^+$/$[L\text{-}H]^-$), their sodium adducts (e.g. $[L + Na]^+$, $[2L + Na]^{+/-}$) and various higher-mass clusters were observed, without clearly identifiable, reproducible Pb(II)-containing ions analogous to those detected for Cu(II). This behaviour is markedly different from that of pyrrole-based diazocrowns, for which high-resolution ESI-MS data showed intense, well-defined groups of peaks that could be fitted to Pb(II)–ligand cluster ions of the type $[2L^-][L][2\ Pb^{2+}][ClO_4^-]$ and related triple-decker species, fully consistent with a 3:2 L:Pb stoichiometry in solution [47]. In the present imidazole-based systems, the absence of analogous Pb(II)–ligand ions in LR-ESI-MS therefore most likely reflects

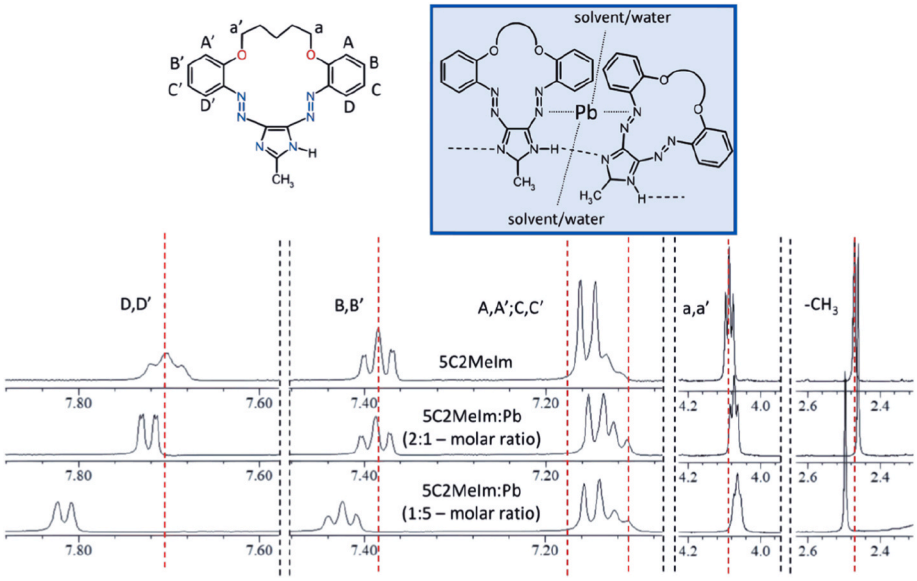

Fig. 20. ^{1}H NMR spectra of **5C2MeIm** and its lead(II) complexes (acetonitrile-d_3); in a blue frame plausible model of lead(II) bindingincluding possible interactions with solvent and/or water molecules. (For interpretation of the references to colour in this figure legend, the reader is referred to the Web version of this article.)

Table 3
^{1}H NMR data for **5C2MeIm** and its lead(II) perchlorate complexes in acetonitrile-d_3;
$\Delta\delta = \delta_{complex} - \delta_{"free" crown}$; shifts in [ppm].

Proton assignment	5C2MeIm		
		crown:lead(II) (Δδ)	
	"free" crown	2:1	1:5
N–H	10.654, bs	10.999, bs (+0.354)	n.d.
-CH$_3$	2.470, s	2.460, s (−0.01)	2.496, s (+0.026)
a,a'	4.086, t	4.072, t (−0.014)	4.063, t (−0.027)
A,A' + C,C'	7.112-7.179, m	7.097-7.169, m (−0.015, −0.01)	7.090-7.176, m (−0.022,-0.003)
B,B′	7.385, t	7.388, t (n.c)	7.424, t (+0.039)
D,D′	7.703, dd, un	7.723, dd (+0.001)	7.816, d (+0.113)

n.d. – not detectable,n.c. – no changes, s – singlet, d – doublet, t – triplet, dd – doublet of doublets, m – multiplet, un – unresolved.

the higher lability and/or gas-phase fragmentation of their Pb(II) complexes under the conditions used, rather than the lack of Pb(II) binding in solution. This conclusion is supported by UV-Vis titrations and Job plots, as well as by systematic ^{1}H NMR chemical shift changes and signal splitting observed upon Pb(II) addition.

Overall, our LR-ESI-MS experiments confirm the formation of Cu(II)–ligand adducts of **5C2MeIm** and **3O2MeIm** and reveal several Cu-containing ions compatible with 1:1, 2:1 and 3:2 L:Cu compositions, but they do not provide simple, well-defined Pb(II)–ligand ions under the conditions employed. This situation is in line with literature reports showing that ESI-MS of Pb(II) complexes can be difficult to interpret and highly sensitive to ionization conditions. For example, Zhang et al. [91] found that negative-mode ESI-MS in methanol is suitable for disulfonamide ligands, but not for their Pb(II) complexes, and that only after deliberate modification of the medium (addition of NaOAc) clearly detectable Pb-containing ions appear. More generally, it is well recognized that ESI-MS spectra of coordination and organometallic compounds may be significantly altered by gas-phase association, dissociation and fragmentation processes and therefore do not always faithfully reflect solution speciation [92]. Therefore the absence of distinct Pb(II)–ligand adducts in our LR-ESI-MS spectra is best interpreted as a consequence of the lability and fragmentation of the imidazole-based Pb(II) complexes under the chosen conditions, rather than as evidence against Pb(II) binding in solution.

3.6. Summary: metal cation complex formation

Affinity towards heavy metal cations of macrocycles **3O2MeIm** and **5C2MeIm** is in agreement with the presence and arrangement of oxygen and nitrogen donor atoms. It might be also explained by the high affinity of copper(II) to N,N-chelating systems [93]. Such arrangement of donor atoms was also utilised in the functionalisation of the polymeric resin with imidazole moieties for selective copper(II) uptake [94]. Thus it might be assumed that copper(II) complex with investigated here macrocycles is formed via metal coordination by nitrogen of azo group and imidazole nitrogen atom. Imidazole and its derivatives are known to form complexes with metal cations via its pyridine-like nitrogen atom or by pyrrole-like one [95,96]. The engagement of imidazole moiety in copper(II) complex formation was also confirmed for several ligands [97]. 1-Alkyl-2-methylimidazoles were investigated as components of polymer inclusion membranes (PIMs) for transport of metal cations [98,99]. Macrocyclic derivatives bearing imidazole residue synthesised in Biernat's group, and also by us, were tested as dopants of PIMs for selective transport of metal cations [100,101].

For a series of azoimidazole ligands, the ability to form complexes with metal cations suggested potential application as metallochromic indicators/extractants for metal cations [95]. It was also proved that in azoimidazole derivatives nitrogen atoms of azo and imidazole moieties are engaged in complex formation [102–104].

The formation of mixed ligand complexes in solution under UV-Vis titration conditions might be associated with the affinity of the Cu(II) and Pb(II) for both the donating nitrogen and the oxygen atoms of investigated macrocyclic ligands [96,105].

3.7. Computational insight into structure–property relationships

The influence of the cavity size and electronic structure on the absorption properties of the macrocycles was analysed using DFT calculations. The calculated UV-Vis spectra (Fig. 21) correspond well with the experimentally determined band positions (acetonitrile) and clearly show that the lowest-energy bands of the 4-methylimidazole derivatives (**3O4MeIm,** λ = 503 nm; **5C4MeIm,** λ = 506 nm) are more shifted to

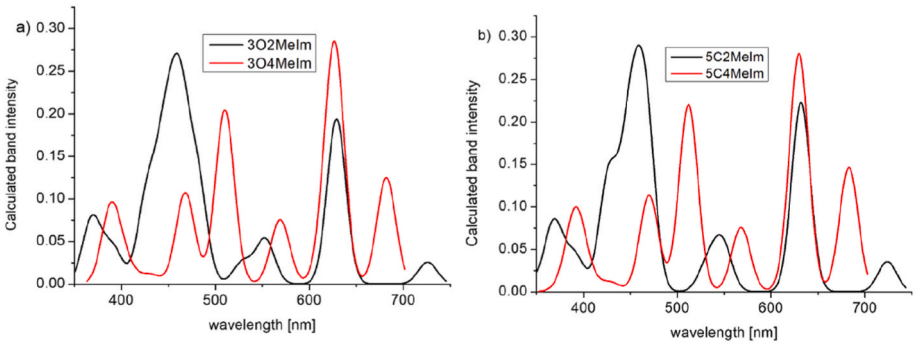

Fig. 21. Calculated UV-Vis spectra of imidazole-based macrocycles: a) **3O2MeIm** (black) and **3O4MeIm** (red); b) **5C2MeIm** (black) and **5C4MeIm** (red). (For interpretation of the references to colour in this figure legend, the reader is referred to the Web version of this article.)

longer wavelengths than those of the corresponding 2-methyl analogues (**3O2MeIm**, λ = 463 nm; **5C2MeIm**, λ = 466 nm), in agreement with the experimentally determined longwave absorption band values.

This trend is fully consistent with our previous study on imidazole-based azomacrocycles, where 4-methylimidazole bearing macrocycles were characterised by a distinct bathochromic shift of the main absorption band compared to the non-substituted imidazole system [37]. In the present series, replacing 4-methylimidazole by 2-methylimidazole reverses this effect and results in a systematic hypsochromic shift of the position of the longwave of absorption band, reflecting both the smaller macrocyclic cavity and the larger HOMO–LUMO gap of the 2-methyl derivatives.

Analysis of the frontier molecular orbitals shows that the lowest-energy transitions are dominated by a HOMO→LUMO excitation with charge-transfer character from the aryl/imidazole fragment towards the cavity region (Fig. 22).

The optimised geometries clearly show that moving the methyl substituent from position 4 to 2 in the imidazole ring and replacing the

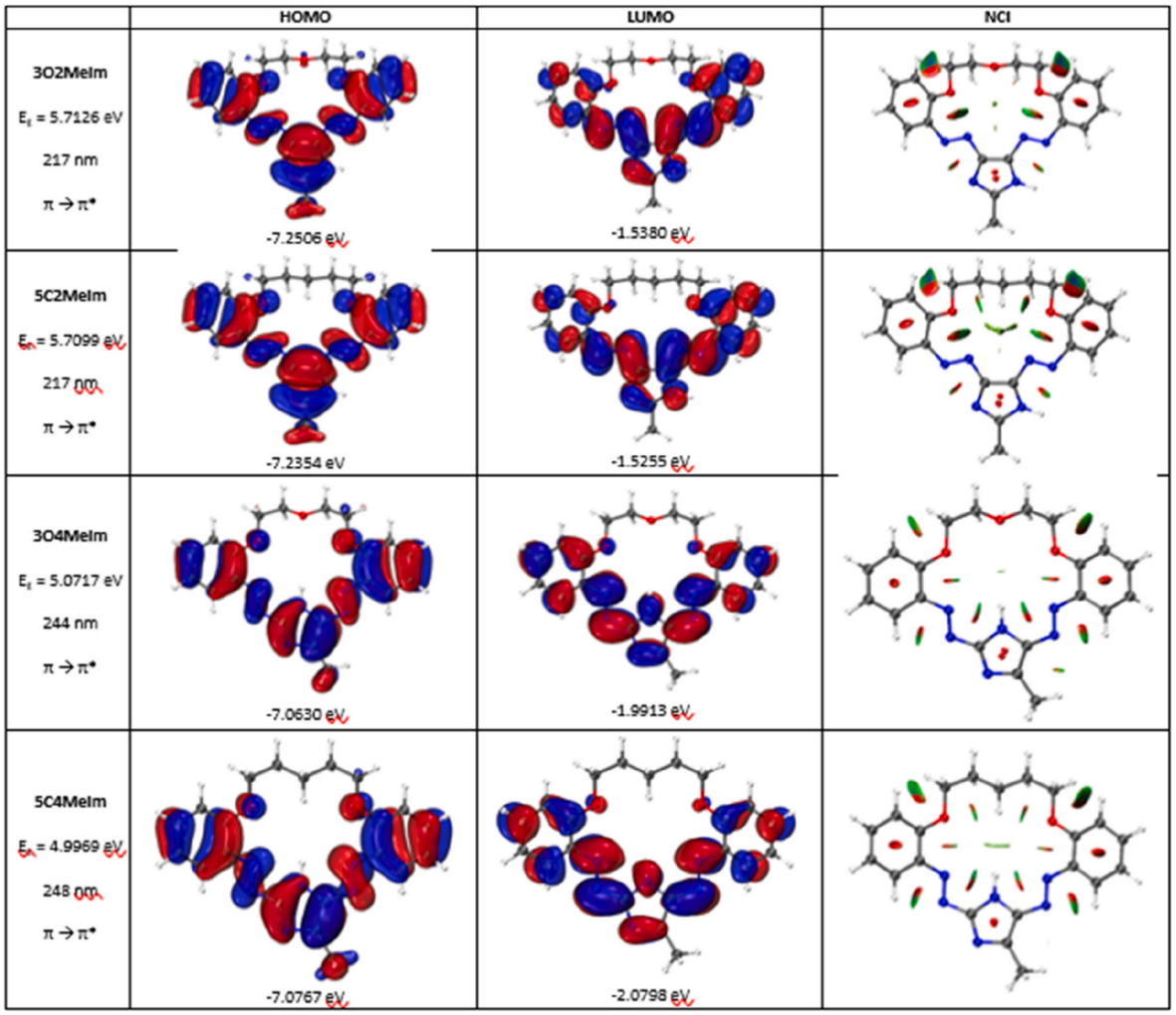

Fig. 22. Frontier molecular orbitals (HOMO and LUMO) and non-covalent interaction (NCI) plots for **3O2MeIm**, **5C2MeIm**, **3O4MeIm** and **5C4MeIm** calculated at the CAM-B3LYP/def2-TZVP level with CPCM (acetonitrile).

oligoether spacer with a hydrocarbon chain leads to a more open cavity, which is reflected in the systematic increase of the O···O distance across the gap from 4.71 Å for **3O2MeIm** to 4.86 Å for **3O4MeIm** and from 4.91 Å for **5C2MeIm** to 5.07 Å for **5C4MeIm** (Fig. 23).

For these four model systems, the calculated HOMO and LUMO energies reveal that the 4-methyl derivatives and the carbon-bridged macrocycle possess a smaller HOMO–LUMO gap than their 2-methyl and oxygen-bridged counterparts, in agreement with the red-shift of the longest wavelength absorption band observed experimentally for the whole series of receptors and with the trends previously reported for related imidazole-based azomacrocycles [37]. The frontier molecular orbitals indicate that the lowest-energy transitions correspond to a HOMO→LUMO excitation with pronounced π→π* charge-transfer character from the aryl/imidazole fragment towards the cavity region, while the associated NCI plots display a continuous belt of weak attractive interactions along the inner rim of the macrocycle, more extended in the 4-methyl receptors and in the carbon-bridged system. Taken together, the evolution of the O···O distance, the reduction of the HOMO–LUMO gap and the redistribution of electron density towards the cavity provide a consistent explanation for the batochromic shifts and changes in colour intensity observed upon structural modification, and place the present receptors within a broader structure–property framework established for imidazole-based chromogenic azomacrocycles.

3.8. Sensing layers

To compare the chromoionophoric properties of **3O2meIm** and **5C2MeIm** upon their immobilisation in sensing layers of optical sensors, we used several materials: cellulose triacetate (CTA), cellulose and glass modified with polystyrene (PG-PS) as a matrix. The first attempt was to test sensing materials in qualitative probes—immersing of sensing material into 0.1 M solution of metal nitrates prepared in nitric acid (10^{-3} M). Colour changes of CTA and PG-PS based materials in quantitative probes are shown in Fig. 24.

Orange-yellow material was found to change colour into brownish-purple depending on the metal nitrate. The most observable colour changes were seen upon interaction with heavy metal nitrates. The colour change of the obtained receptor layers presented as the parameter ΔE_{RGB} is shown in Fig. 25. Colour changes of CTA and PG-PS sensing layers expressed as (R + G + B)/3 and I = 0.299R + 0.587G + 0.114B are shown in Figure S42 and Figure S43.

Sensing material obtained with the use of cellulose immobilised on glass plates were also characterised by colour changes when immersed into metal nitrates solutions. However, the material obtained via this approach, despite many attempts, was patchy and coloured with the greyish hue (cf. Fig. S44), so it was rejected from further studies.

Colour changes of the obtained sensing materials are more distinct for **3O2MeIm**, however not spectacularly. Also selectivity towards particular metal cation is rather moderate.

Analysing the obtained results, it is well seen that 17-membered macrocyclic azocrowns can be regarded as chromoionophores. However, comparing to previously investigated macrocycles with imidazole/4-methylimidazole [45], the selectivity towards lead(II) and bismuth(III) is lost.

In the present study, the relocation of the methyl substituent to the 2-position in the imidazole ring, resulting in a reduction in macrocyclic cavity size, altered the potential hydrogen-bonding network and influence the lipophilicity of the macrocycle. These structural modifications probably affect the interaction with the solid matrix and influence the chromogenic response, consistent with earlier observations for immobilised azomacrocyclic systems [37,45]. Nevertheless, the preserved optical activity and relative stability of the immobilised layers highlight the robustness of these materials and their potential for fine-tuning through molecular design—particularly by controlled adjustment of cavity geometry and substituent orientation—to achieve improved solid-state colorimetric sensing performance.

3.8.1. Regeneration and reversibility of sensing layers

Regeneration studies were performed to assess the reversibility of the metal-induced colour changes in both CTA-based optodes and PG-PS-supported materials. For CTA membranes, complete regeneration was not achieved with either 0.1 M HNO_3 or 0.1 M EDTA. The most reproducible response was observed for 5C2MeIm in the presence of Cu

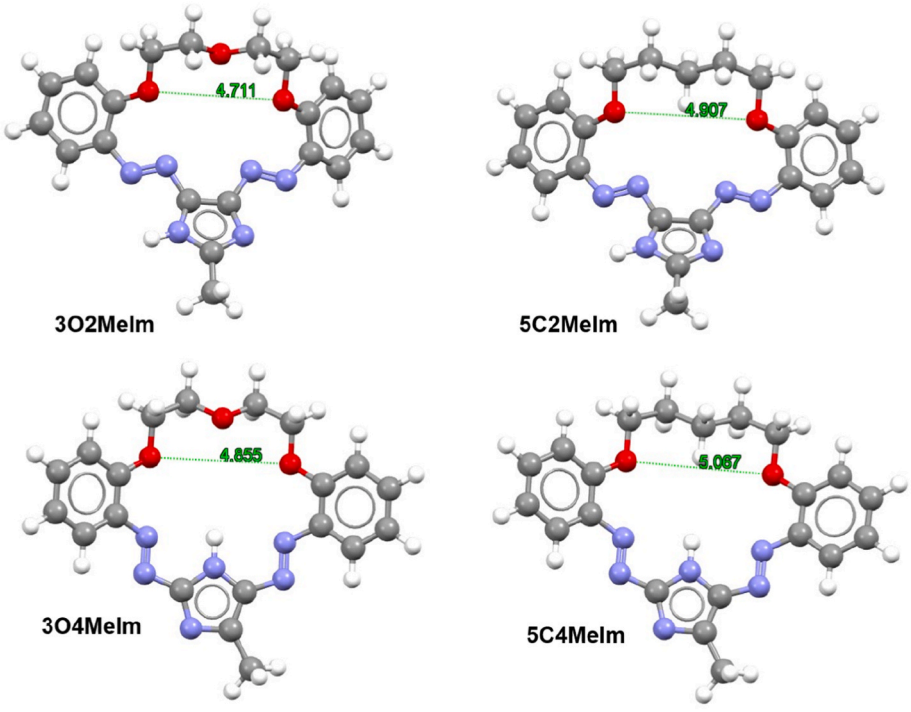

Fig. 23. DFT-optimised geometries of **3O2MeIm**, **3O4MeIm**, **5C2MeIm** and **5C4MeIm** with O···O distances across the cavity.

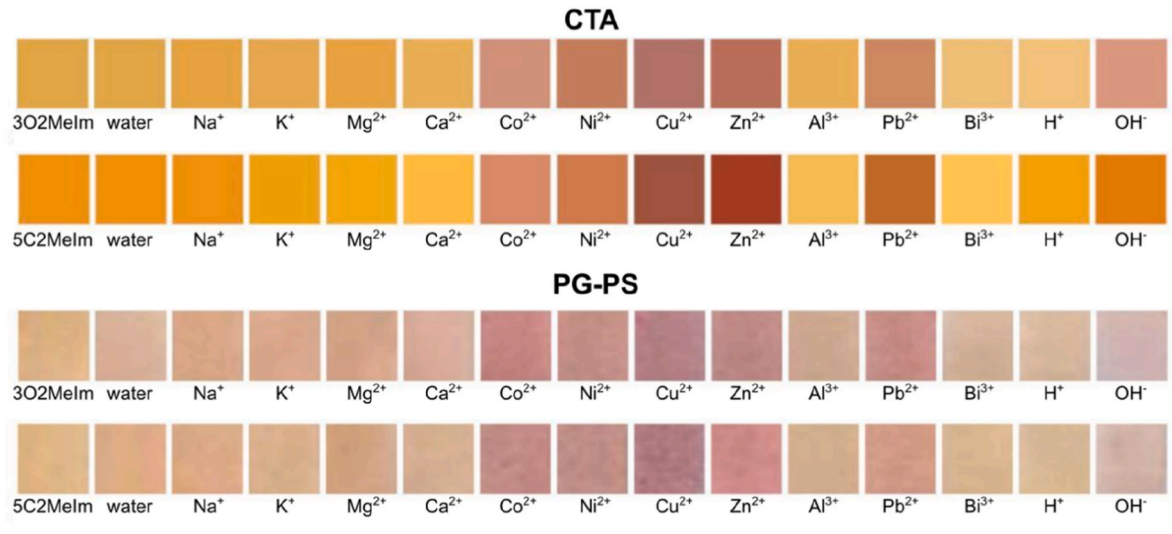

Fig. 24. Colour change of CTA (top) and PG-PS (bottom) based materials with **3O2MeIm** and **5C2MeIm** as chromoionophores upon immersing the material in 0.1 M solution of metal nitrates (nitric acid 10^{-3} M as a solvent) and nitric acid (H^+) and sodium hydroxide (OH^-) solutions. (For interpretation of the references to colour in this figure legend, the reader is referred to the Web version of this article.)

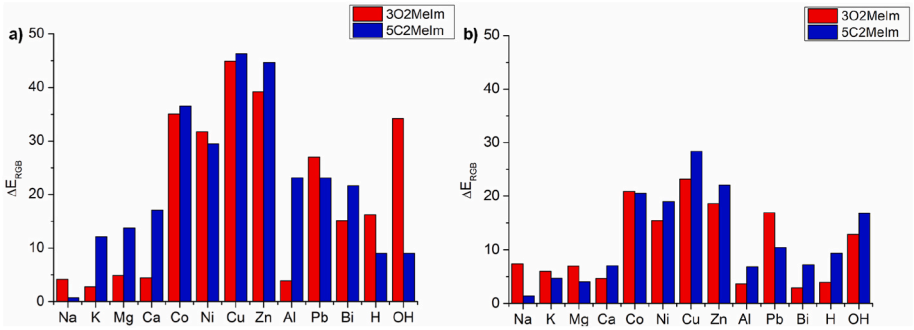

Fig. 25. Comparison of the colour change of: a) CTA and b) PG-PS-based materials with **3O2MeIm** and **5C2MeIm** chromoionophores in 0.1 M aqueous solutions of metal nitrates expressed as ΔE_{RGB} parameter. (For interpretation of the references to colour in this figure legend, the reader is referred to the Web version of this article.)

$(NO_3)_2$, regenerated with HNO_3 (Fig. 26). However, the ΔE_{RGB} parameter decreased by approximately 30% (from 98.31 to 68.95) after five cycles, indicating partial irreversibility or progressive loss of ligand–metal interaction.

For **3O2MeIm**, a noticeable decrease in colour intensity was observed after several cycles, which can be attributed to the gradual leaching of the chromoionophore into solution. This effect was also observed for Pb(II), but to a lesser extent than for Cu(II). The observed leaching of **3O2MeIm** is consistent with previous studies on ion-selective electrodes, where similar leakage was reported [50].

For PG-PS-supported materials, regeneration was even less effective (Fig. 27). In particular, **3O2MeIm** showed significant wash-out in both regenerative solutions, consistent with previous observations for this ligand. Additionally, neither EDTA nor HNO_3 fully restored the original colour of **5C2MeIm**-based materials after one cycle.

These results demonstrate that while partial reversibility of the colour response is achievable, the regeneration efficiency is governed by chromoionophore structure and matrix interactions, which limit long-term reusability under the applied conditions.

In our previous studies on closely related imidazole-based chromoionophores [37,45], efficient regeneration of receptor layers was observed under comparable conditions. The present results therefore clearly illustrate how even subtle structural modifications within the same family of compounds can markedly influence not only metal-binding properties and complex stability, but also the durability and practical reusability of sensing layers.

4. Conclusions

A new, 17-membered bisazomacrocycle bearing 2-methylimidazole (**5C2MeIm**) was successfully synthesised and compared with its oligoether-linked analogue (**3O2MeIm**). The influence of the linker type and the substitution pattern within the imidazole ring on macrocyclisation efficiency and complexation behaviour was evaluated.The relocation of the methyl group from the 4- to the 2-position in the imidazole ring alters the direction of the coupling reaction, leading to a macrocycle of smaller molecular cavity and distinct conformation. These structural consequences, combined with the nature of the spacer, significantly affect the chromogenic response and the type of complexes formed with Pb(II) and Cu(II) ions. In particular, the orientation of the N–H group within the macrocyclic cavity plays a decisive role in determining the colour intensity and metal-binding mode.

These findings extend our previous series on imidazole-based azomacrocycles and refine the understanding of the structure–property relationships governing their chromogenic and ion-recognition behaviour.

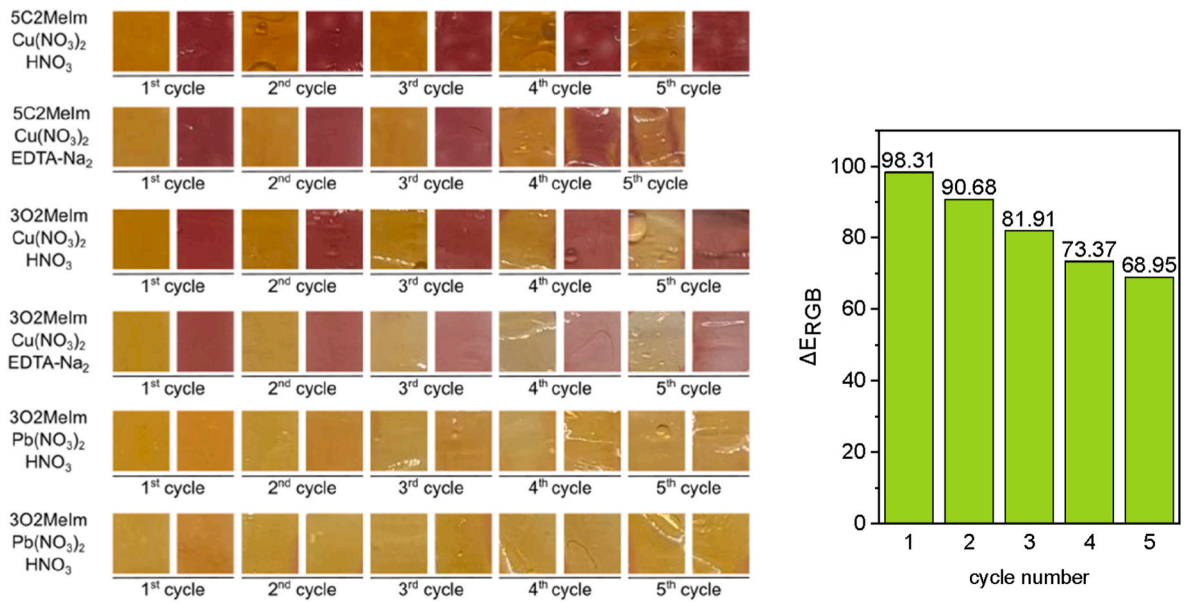

Fig. 26. a) CTA-based optodes with **5C2MeIm** or **3O2MeIm** as chromoionophores, after 5 cycles of immersion in $Cu(NO_3)_2$ or $Pb(NO_3)_2$ solutions (0.1 M) and washing with HNO_3 or EDTA-Na_2 solutions (0.1 M); b) comparison of effectiveness of regeneration in HNO_3 for the receptor layers with **5C2MeIm** in the presence of $Cu(NO_3)_2$ (given as ΔE_{RGB}).

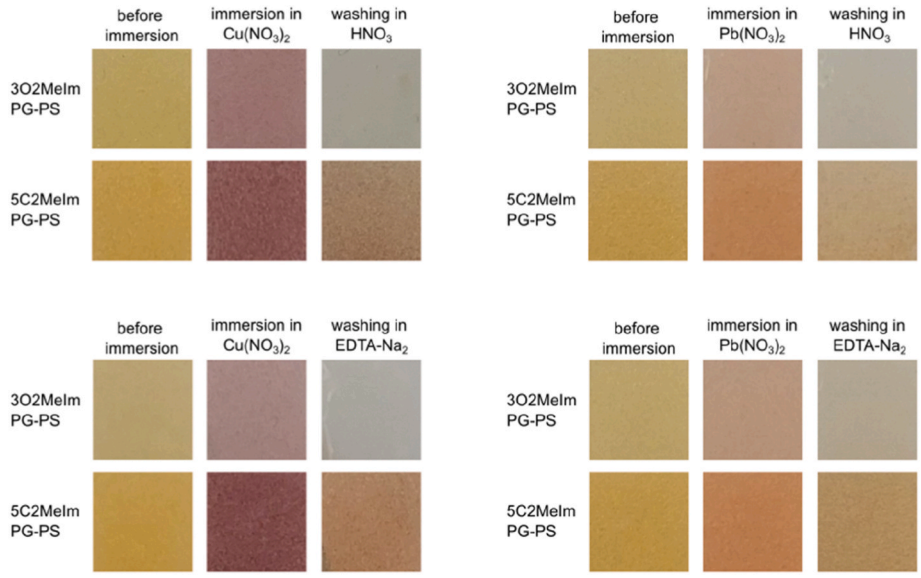

Fig. 27. PG-PS receptor layers with **5C2MeIm** or **3O2MeIm** as chromoionophores, after a cycle of immersion in $Cu(NO_3)_2$ or $Pb(NO_3)_2$ solutions (0.1 M) and washing with HNO_3 or EDTA-Na_2 solutions (0.1 M).

CRediT authorship contribution statement

Paulina Miklaszewska: Writing – review & editing, Writing – original draft, Visualization, Methodology, Investigation, Formal analysis, Data curation, Conceptualization. **Michał Aszyk:** Conceptualization, Data Curation, Investigation, Visualization, Writing – original draft, Writing – review & editing.. **Paweł Sowiński:** Investigation, Writing – original draft. **Andrzej Okuniewski:** Investigation, Writing – original draft. **Zofia Kaczorowska:** Validation, Investigation. **Zuzanna Antonowicz:** Visualization, Investigation. **Gabriela Burakowska:** Visualization, Investigation. **Ewa Wagner-Wysiecka:** Writing – review & editing, Writing – original draft, Visualization, Validation, Supervision, Methodology, Investigation, Funding acquisition, Formal analysis, Data curation, Conceptualization.

Funding sources

Financial support of these studies from Gdańsk University of Technology by the DEC-6/1/2022/IDUB/III.4c/Tc grant under the Technetium Talent Management Grants - 'Excellence Initiative - Research University' program is gratefully acknowledged. This work was supported by the Faculty of Chemistry, Gdańsk University of Technology, No. 037137 - an internal grant from statutory funds.

Declaration of competing interest

The authors declare that they have no known competing financial interests or personal relationships that could have appeared to influence the work reported in this paper.

Acknowledgments

The authors gratefully acknowledge Dr. Olga Ciupak (Gdańsk University of Technology, Faculty of Chemistry, Nuclear Magnetic Resonance Laboratory) for her kind assistance and valuable involvement in the NMR measurements. The Authors would like to thank the anonymous Reviewers for their insightful comments and constructive suggestions, which have significantly improved the quality of the manuscript.

Appendix A. Supplementary data

Supplementary data to this article can be found online at https://doi.org/10.1016/j.dyepig.2026.113696.

Data availability

Data will be made available on request.

References

[1] Tchounwou PB, Yedjou CG, Patlolla AK, Sutton DJ. Heavy metal toxicity and the environment. Exp Suppl 2012;101:133–64. https://doi.org/10.1007/978-3-7643-8340-4_6.
[2] Yadav M, Gupta R, Sharma RK. Green and sustainable pathways for wastewater purification. Adv Water Purif Tech Meet Needs Dev Dev Ctries 2019:355–83. https://doi.org/10.1016/B978-0-12-814790-0.00014-4.
[3] Singh V, Singh N, Rai SN, Kumar A, Singh AK, Singh MP, et al. Heavy metal contamination in the aquatic ecosystem: toxicity and its remediation using eco-friendly approaches. Toxics 2023;11:147. https://doi.org/10.3390/toxics11020147.
[4] Briffa J, Sinagra E, Blundell R. Heavy metal pollution in the environment and their toxicological effects on humans. Heliyon 2020;6:e04691. https://doi.org/10.1016/J.HELIYON.2020.E04691.
[5] Hama Aziz KH, Mustafa FS, Omer KM, Hama S, Hamarawf RF, Rahman KO. Heavy metal pollution in the aquatic environment: efficient and low-cost removal approaches to eliminate their toxicity: a review. RSC Adv 2023;13:17595–610. https://doi.org/10.1039/D3RA00723E.
[6] Kaur R, Kaur H, Sharma A. Uptake and toxicity of heavy metals: the protective frontiers of metal binding proteins. J Geochem Explor 2025;271:107673. https://doi.org/10.1016/j.gexplo.2025.107673.
[7] Sperdouli I. Heavy metal toxicity effects on plants. Toxics 2022;10:715. https://doi.org/10.3390/toxics10120715.
[8] Tahir I, Alkheraije KA. A review of important heavy metals toxicity with special emphasis on nephrotoxicity and its management in cattle. Front Vet Sci 2023;10:1149720. https://doi.org/10.3389/fvets.2023.1149720.
[9] Das S, Sultana KW, Ndhlala AR, Mondal M, Chandra I. Heavy metal pollution in the environment and its impact on health: exploring green technology for remediation. Environ Health Insights 2023;17:11786302231201260. https://doi.org/10.1177/11786302231201259.
[10] Balali-Mood M, Naseri K, Tahergorabi Z, Khazdair MR, Sadeghi M. Toxic mechanisms of five heavy metals: Mercury, lead, chromium, cadmium, and arsenic. Front Pharmacol 2021;12:643972. https://doi.org/10.3389/fphar.2021.643972.
[11] Izydorczyk G, Mikula K, Skrzypczak D, Moustakas K, Witek-Krowiak A, Chojnacka K. Potential environmental pollution from copper metallurgy and methods of management. Environ Res 2021;197:111050. https://doi.org/10.1016/J.ENVRES.2021.111050.
[12] Hussain S, Khan M, Sheikh TMM, Mumtaz MZ, Chohan TA, Shamim S, et al. Zinc essentiality, toxicity, and its bacterial bioremediation: a comprehensive insight. Front Microbiol 2022;13:900740. https://doi.org/10.3389/fmicb.2022.900740.
[13] Hordyjewska A, Popiołek Ł, Kocot J. The many "faces" of copper in medicine and treatment. Biometals 2014;27:611–21. https://doi.org/10.1007/s10534-014-9736-5.
[14] Takahashi A. Role of zinc and copper in erythropoiesis in patients on hemodialysis. J Ren Nutr 2022;32:650–7. https://doi.org/10.1053/J.JRN.2022.02.007.
[15] Gromadzka G, Tarnacka B, Flaga A, Adamczyk A. Copper dyshomeostasis in neurodegenerative Diseases—Therapeutic implications. Int J Mol Sci 2020;21:9259. https://doi.org/10.3390/ijms21239259.
[16] Chen Z, Li Y yuan, Liu X. Copper homeostasis and copper-induced cell death: novel targeting for intervention in the pathogenesis of vascular aging. Biomed Pharmacother 2023;169:115839. https://doi.org/10.1016/J.BIOPHA.2023.115839.
[17] Grubman A, White AR. Copper as a key regulator of cell signalling pathways. Expet Rev Mol Med 2014;16:e11. https://doi.org/10.1017/erm.2014.11.
[18] Myint ZW, Oo TH, Thein KZ, Tun AM, Saeed H. Copper deficiency anemia: review article. Ann Hematol 2018;97:1527–34. https://doi.org/10.1007/s00277-018-3407-5.
[19] Moon N, Aryan M, Westerveld D, Nathoo S, Glover S, Kamel AY. Clinical manifestations of copper deficiency: a case report and review of the literature. Nutr Clin Pract 2021;36:1080–5. https://doi.org/10.1002/ncp.10582.
[20] Tahir N, Ashraf A, Bin Waqar SH, Rafae A, Kantamneni L, Sheikh T, et al. Copper deficiency, a rare but correctable cause of pancytopenia: a review of literature. Expert Rev Hematol 2022;15:999–1008. https://doi.org/10.1080/17474086.2022.2142113.
[21] Wang Z, Jin D, Zhou S, Dong N, Ji Y, An P, et al. Regulatory roles of copper metabolism and cuproptosis in human cancers. Front Oncol 2023;13:1123420. https://doi.org/10.3389/fonc.2023.1123420.
[22] Lelièvre P, Sancey L, Coll J-L, Deniaud A, Busser B. The multifaceted roles of copper in cancer: a trace metal element with dysregulated metabolism, but also a target or a bullet for therapy. Cancers (Basel) 2020;12:3594. https://doi.org/10.3390/cancers12123594.
[23] Guan D, Zhao L, Shi X, Ma X, Chen Z. Copper in cancer: from pathogenesis to therapy. Biomed Pharmacother 2023;163:114791. https://doi.org/10.1016/J.BIOPHA.2023.114791.
[24] An Y, Li S, Huang X, Chen X, Shan H, Zhang M. The role of copper homeostasis in brain disease. Int J Mol Sci 2022;23:13850. https://doi.org/10.3390/ijms232213850.
[25] Kaler SG. Inborn errors of copper metabolism. Handb Clin Neurol 2013;113:1745–54. https://doi.org/10.1016/B978-0-444-59565-2.00045-9.
[26] Rădulescu A, Lundgren S. A pharmacokinetic model of lead absorption and calcium competitive dynamics. Sci Rep 2019;9:14225. https://doi.org/10.1038/s41598-019-50654-7.
[27] Mason LH, Harp JP, Han DY. Pb neurotoxicity: neuropsychological effects of lead toxicity. BioMed Res Int 2014;2014:1–8. https://doi.org/10.1155/2014/840547.
[28] Landrigan PJ. Lead and the heart: an ancient metal's contribution to modern disease. Lancet Public Health 2018;3:e156–7. https://doi.org/10.1016/S2468-2667(18)30043-4.
[29] Wei W, Wu X, Bai Y, Li G, Feng Y, Meng H, et al. Lead exposure and its interactions with oxidative stress polymorphisms on lung function impairment: results from a longitudinal population-based study. Environ Res 2020;187:109645. https://doi.org/10.1016/j.envres.2020.109645.
[30] World Health Organization. Lead poisoning. https://WwwWhoInt/News-Room/Fact-Sheets/Detail/Lead-Poisoning-and-Health n.d.
[31] Ungureanu EL, Mocanu AL, Stroe CA, Duță DE, Mustățea G. Assessing health risks associated with heavy metals in food: a bibliometric analysis. Foods 2023;12:3974. https://doi.org/10.3390/foods12213974.
[32] Pujol L, Evrard D, Groenen-Serrano K, Freyssinier M, Ruffien-Cizsak A, Gros P. Electrochemical sensors and devices for heavy metals assay in water: the French groups' contribution. Front Chem 2014;2:19. https://doi.org/10.3389/fchem.2014.00019.
[33] Bereza-Malcolm LT, Mann G, Franks AE. Environmental sensing of heavy metals through whole cell microbial biosensors: a synthetic biology approach. ACS Synth Biol 2015;4:535–46. https://doi.org/10.1021/sb500286r.
[34] Velusamy K, Periyasamy S, Kumar PS, Rangasamy G, Nisha Pauline JM, Ramaraju P, et al. Biosensor for heavy metals detection in wastewater: a review. Food Chem Toxicol 2022;168:113307. https://doi.org/10.1016/J.FCT.2022.113307.
[35] Mistlberger G, Crespo GA, Bakker E. Ionophore-based optical sensors. Annu Rev Anal Chem 2014;7:483–512. https://doi.org/10.1146/annurev-anchem-071213-020307.
[36] Müller R, Anders N, Titus J, Enke D. Ultra-thin porous glass membranes—An innovative material for the immobilization of active species for optical chemosensors. Talanta 2013;107:255–62. https://doi.org/10.1016/j.talanta.2012.12.038.
[37] Galiński B, Chojnacki J, Szwarc-Karabyka K, Małkowski A, Sopel D, Zwolińska A, et al. Chromogenic azomacrocycles with imidazole residue: structure vs. properties. Dyes Pigments 2023;219:111610. https://doi.org/10.1016/J.DYEPIG.2023.111610.
[38] Liu X, Naraginti S, Zhang F, Sathishkumar K, Subramaniam V, Ramachandran K, et al. Selective detection and quantification of Co2+ ions by mesoscopic engineering silica-monolithic based circular optical strips. J Environ Chem Eng 2025;13:115671. https://doi.org/10.1016/j.jece.2025.115671.
[39] Oehme I, Wolfbeis OS. Optical sensors for determination of heavy metal ions. Mikrochim Acta 1997;126:177–92. https://doi.org/10.1007/BF01242319.
[40] Burratti L, Sgreccia E, Bertelà F, Galiano F. Metal nanostructures in polymeric matrices for optical detection and removal of heavy metal ions, pesticides and dyes from water. Chemosphere 2024;362:142636. https://doi.org/10.1016/j.chemosphere.2024.142636.
[41] Pedugu Sivaraman S, Srinivasan P, Madhu DK, Deivasigamani P, Mohan AM. Probe-infused polymer monolithic sensor for colorimetric detection of Pb2+ in environmental water samples and tobacco extracts. J Hazard Mater 2025;487:137247. https://doi.org/10.1016/j.jhazmat.2025.137247.
[42] Eid S, Abdelwahab AA, Amin AS, El-Feky HH. An innovative eco-friendly optical sensor designed specifically to detect lanthanum ions in environmental samples. Spectrosc Lett 2025:1–14. https://doi.org/10.1080/00387010.2025.2482732.
[43] El-Bahy SM, Amin AS, El-Sayed R, Debbabi KF, Hassan N, Aish M. Utilization of non-plasticized polymer inclusion membrane for highly selective colorimetric sensor detection of zirconium in environmental samples. RSC Adv 2025;15:5462–75. https://doi.org/10.1039/D4RA05674D.
[44] Singh A, Shah SS, Sharma C, Gupta V, Sundramoorthy AK, Kumar P, et al. An approach towards different techniques for detection of heavy metal ions and their removal from waste water. J Environ Chem Eng 2024;12:113032. https://doi.org/10.1016/j.jece.2024.113032.

[45] Galiński B, Wagner-Wysiecka E. Macrocyclic derivatives of imidazole as chromoionophores for bismuth(III)/lead(II) pair. Sensors Actuators B Chem 2024; 399:134798. https://doi.org/10.1016/J.SNB.2023.134798.

[46] Galiński B, Chojnacki J, Wagner-Wysiecka E. Simple colorimetric copper(II) sensor – spectral characterization and possible applications. Spectrochim Acta Part A Mol Biomol Spectrosc 2023;293:122472. https://doi.org/10.1016/J.SAA.2023.122472.

[47] Galiński B, Luboch E, Chojnacki J, Wagner-Wysiecka E. Novel diazocrowns with pyrrole residue as Lead(II)Colorimetric probes. Materials (Basel) 2021;14:7239. https://doi.org/10.3390/ma14237239.

[48] Galiński B, Wagner-Wysiecka E. Pyrrole bearing diazocrowns: selective chromoionophores for lead(II) optical sensing. Sensors Actuators B Chem 2022; 361:131678. https://doi.org/10.1016/J.SNB.2022.131678.

[49] Wagner-Wysiecka E, Luboch E, Kowalczyk M, Biernat JF. Chromogenic macrocyclic derivatives of azoles—synthesis and properties. Tetrahedron 2003; 59:4415–20. https://doi.org/10.1016/S0040-4020(03)00618-5.

[50] Wagner-Wysiecka E, Jamrógiewicz M, Fonari MS, Biernat JF. Azomacrocyclic derivatives of imidazole: synthesis, structure, and metal ion complexation properties. Tetrahedron 2007;63:4414–21. https://doi.org/10.1016/J.TET.2007.03.095.

[51] Dinten O, Spichiger UE, Chaniotakis N, Gehrig P, Rusterholz B, Morf WE, et al. Lifetime of neutral-carrier-based liquid membranes in aqueous samples and blood and the lipophilicity of membrane components. Anal Chem 1991;63:596–603. https://doi.org/10.1021/ac00006a009.

[52] Kyvala M, Lukes I. Program package "OPIUM.". 2000. n.d.

[53] Perera WN, Hefter G, Sipos PM. An investigation of the Lead(II)−Hydroxide system. Inorg Chem 2001;40:3974–8. https://doi.org/10.1021/ic001415o.

[54] Liu Q, Liu Y. Distribution of Pb(II) species in aqueous solutions. J Colloid Interface Sci 2003;268:266–9. https://doi.org/10.1016/S0021-9797(03)00638-6.

[55] ImageJ. https://ImagejNet/Ij/n.d.

[56] Vidal E, Lorenzetti AS, Garcia CD, Domini CE. Use of universal 3D-Printed smartphone spectrophotometer to develop a time-based analysis for hypochlorite. Anal Chim Acta 2021;1151:338249. https://doi.org/10.1016/j.aca.2021.338249.

[57] Wagner-Wysiecka E, Rzymowski T, Fonari MS, Kulmaczewski R, Luboch E. Pyrrole azocrown ethers—synthesis, crystal structures, and fluorescence properties. Tetrahedron 2011;67:1862–72. https://doi.org/10.1016/j.tet.2011.01.027.

[58] Brown RD, Duffin HC, Maynard JC, Ridd 805 JH. The mechanism of the coupling of diazonium salts with heterocyclic compounds. Part I. Glyoxaline. J Chem Soc 1953;3937. https://doi.org/10.1039/jr9530003937.

[59] Jamrógiewicz M, Sadowska K, Biernat JF. Effect of cyclodextrins on coupling of o-Ethoxybenzenediazonium salt with pyrrole, imidazole and 2-Methylimidazole. J Inclusion Phenom Macrocycl Chem 2006;56:355–62. https://doi.org/10.1007/s10847-006-9115-0.

[60] Sadowska K, Jamrógiewicz M, Biernat JF. Stimulated by cyclodextrins high yield synthesis of azocrown analogues comprising pyrrole or imidazole residues. Supramol Chem 2008;20:717–22. https://doi.org/10.1080/10610270701767311.

[61] Cid-Samamed A, Rakmai J, Mejuto JC, Simal-Gandara J, Astray G. Cyclodextrins inclusion complex: preparation methods, analytical techniques and food industry applications. Food Chem 2022;384:132467. https://doi.org/10.1016/j.foodchem.2022.132467.

[62] Waters LJ, Bedford S, Parkes GMB, Mitchell JC. Influence of lipophilicity on drug–cyclodextrin interactions: a calorimetric study. Thermochim Acta 2010;511: 102–6. https://doi.org/10.1016/j.tca.2010.07.031.

[63] Hachuła B, Nowak M, Kusz J. Crystal and molecular structure analysis of 2-Methylimidazole. J Chem Crystallogr 2010;40:201–6. https://doi.org/10.1007/s10870-009-9634-9.

[64] Daina A, Michielin O, Zoete V. SwissADME: a free web tool to evaluate pharmacokinetics, drug-likeness and medicinal chemistry friendliness of small molecules. Sci Rep 2017;7:42717. https://doi.org/10.1038/srep42717.

[65] McGowan JC, Sowada R. Characteristic volumes and properties of surfactants. J Chem Technol Biotechnol 1993;58:357–61. https://doi.org/10.1002/jctb.280580408.

[66] Nollet M, Boulghobra H, Calligaro E, Rodier J-D. An efficient method to determine the Hydrophile-Lipophile Balance of surfactants using the phase inversion temperature deviation of C i E j/n -octane/water emulsions. Int J Cosmet Sci 2019;41:99–108. https://doi.org/10.1111/ics.12516.

[67] Wicha-Komsta K, Komsta Ł. Unconventional TLC systems in lipophilicity determination: a review. J Liq Chromatogr Relat Technol 2017;40:219–25. https://doi.org/10.1080/10826076.2017.1298023.

[68] Milojković-Opsenica D, Andrić F, Šegan S, Trifković J, Tešić Ž. Thin-layer chromatography in quantitative structure-activity relationship studies. J Liq Chromatogr Relat Technol 2018;41:272–81. https://doi.org/10.1080/10826076.2018.1447892.

[69] Chen D, Zhao M, Tan W, Li Y, Li X, Li Y, et al. Effects of intramolecular hydrogen bonds on lipophilicity. Eur J Pharmaceut Sci 2019;130:100–6. https://doi.org/10.1016/J.EJPS.2019.01.020.

[70] Loehr HG, Voegtle F. Chromo- and fluoroionophores. A new class of dye reagents. Acc Chem Res 1985;18:65–72. https://doi.org/10.1021/ar00111a001.

[71] Chapoteau E, Czech BP, Zazulak W, Kumar A. First practical colorimetric assay of lithium in serum. Clin Chem 1992;38:1654–7. https://doi.org/10.1093/clinchem/38.9.1654.

[72] Sandanayake KRAS, Sutherland IO. Organic dyes for optical sensors. Sensors Actuators B Chem 1993;11:331–40. https://doi.org/10.1016/0925-4005(93)85272-C.

[73] Wagner-Wysiecka E, Skwierawska A, Kravtsov VC, Biernat JF. New class of chromogenic proton-dissociable azocrown reagents for alkali metal ions. J Supramol Chem 2001;1:77–85. https://doi.org/10.1016/S1472-7862(01)00014-4.

[74] Suryanti V, Wibowo FR, Marzuki A, Sari MRK. Cation sensing capabilities of A nitrophenyl cinnamaldehyde derivative. Molekul 2020;15:191. https://doi.org/10.20884/1.jm.2020.15.3.654.

[75] Arif Z, Sugiarti S, Rohaeti E, Batubara I. A sensor (Optode) based on cellulose triacetate membrane for Fe(III) detection in water samples. Chemistry (Easton) 2023;6:81–94. https://doi.org/10.3390/chemistry6010005.

[76] Rajpurohit D, Sharma P, Bathvar H, Syed S, Shrivastav PS. Lithium selective receptors. Coord Chem Rev 2024;515:215968. https://doi.org/10.1016/j.ccr.2024.215968.

[77] Gordon PF, Gregory P. Organic chemistry in colour. Berlin, Heidelberg: Springer Berlin Heidelberg; 1987. https://doi.org/10.1007/978-3-642-82959-8.

[78] Panuszko A, Bruździak P, Śmiechowski M, Stasiulewicz M, Stefaniak J, Stangret J. DMSO hydration redefined: unraveling the hydrophobic hydration of solutes with a mixed hydrophilic–hydrophobic characteristic. J Mol Liq 2019;294:111661. https://doi.org/10.1016/j.molliq.2019.111661.

[79] Hazra MK, Bagchi B. Non-equilibrium solvation dynamics in water-DMSO binary mixture: composition dependence of non-linear relaxation. J Chem Phys 2018; 149. https://doi.org/10.1063/1.5036689.

[80] Senac C, Desgranges S, Contino-Pépin C, Urbach W, Fuchs PFJ, Taulier N. Effect of Dimethyl sulfoxide on the binding of 1-Adamantane carboxylic acid to β- and γ-Cyclodextrins. ACS Omega 2018;3:1014–21. https://doi.org/10.1021/acsomega.7b01212.

[81] Koley S, Ghosh S. Study of microheterogeneity in acetonitrile–water binary mixtures by using polarity-resolved solvation dynamics. ChemPhysChem 2015; 16:3518–26. https://doi.org/10.1002/cphc.201500663.

[82] Koley S, Ghosh S. A deeper insight into an intriguing acetonitrile–water binary mixture: synergistic effect, dynamic Stokes shift, fluorescence correlation spectroscopy, and NMR studies. Phys Chem Chem Phys 2016;18:32308–18. https://doi.org/10.1039/C6CP05024G.

[83] Nagaj J, Stokowa-Sołtys K, Kurowska E, Frączyk T, Jeżowska-Bojczuk M, Bal W. Revised coordination model and stability constants of Cu(II) complexes of Tris Buffer. Inorg Chem 2013;52:13927–33. https://doi.org/10.1021/ic401451s.

[84] Gozdas S, Kose M, Mckee V, Elmastas M, Demirtas I, Kurtoglu M. Crystal structures, electronic spectra and anticancer properties of new azo-azomethines and their nickel(II) and copper(II) chelates. J Mol Struct 2024;1304:137691. https://doi.org/10.1016/j.molstruc.2024.137691.

[85] Al-Adilee KJ, Jawad SH, Kyhoiesh HAK, Hassan HM. Synthesis, characterization, biological applications, and molecular docking studies of some transition metal complexes with azo dye ligand derived from 5-methyl imidazole. J Mol Struct 2024;1295:136695. https://doi.org/10.1016/j.molstruc.2023.136695.

[86] Al-Adilee K, Kyhoiesh HAK. Preparation and identification of some metal complexes with new heterocyclic azo dye ligand 2-[2 – - (1- Hydroxy -4- Chloro phenyl) azo]- imidazole and their spectral and thermal studies. J Mol Struct 2017;1137:160–78. https://doi.org/10.1016/j.molstruc.2017.01.054.

[87] Sarker KK, Jana AD, Mostafa G, Wu J-S, Lu T-H, Sinha C. Iodo bridged lead(II) compounds of azoimidazoles: Single crystal X-ray structures of [di-iodo-{1-methyl-2-(p-tolylazo)imidazole}lead(II)]n and {1-methyl-3-benzyl-2-(p-tolylazo) imidazolium}m-{tri-iodoplumbate(II)}m. Inorg Chim Acta 2006;359:4377–85. https://doi.org/10.1016/j.ica.2006.05.037.

[88] Misra TK, Das D, Sinha C. Chemistry of azoimidazoles: synthesis, spectral characterization and redox properties ofbis(N(1)-alkyl-2-(arylazo)imidazole) copper (I) and silver(I) complexes. Polyhedron 1997;16:4163–70. https://doi.org/10.1016/S0277-5387(97)00127-7.

[89] Hodgson JB, Percy (the late) Gordon C, Thornton DA. The infrared spectra of imidazole complexes of first transition series metal(ii) nitrates and perchlorates. J Mol Struct 1980;66:81–92. https://doi.org/10.1016/0022-2860(80)80161-X.

[90] Lane TJ, Nakagawa I, Walter JL, Kandathil AJ. Infrared investigation of certain imidazole derivatives and their metal chelates. Inorg Chem 1962;1:267–76. https://doi.org/10.1021/ic50002a014.

[91] Zhang W, Cai Y, Kavallieratos K. Investigation of disulfonamide ligands derived from o -phenylenediamine and their Pb(II) complexes by electrospray ionization mass spectrometry. Rapid Commun Mass Spectrom 2006;20:303–8. https://doi.org/10.1002/rcm.2312.

[92] McIndoe JS, Vikse KL. Assigning the ESI mass spectra of organometallic and coordination compounds. J Mass Spectrom 2019;54:466–79. https://doi.org/10.1002/jms.4359.

[93] Peña Q, Sciortino G, Maréchal J-D, Bertaina S, Simaan AJ, Lorenzo J, et al. Copper(II) N , N , O -Chelating Complexes as Potential Anticancer agents. Inorg Chem 2021;60:2939–52. https://doi.org/10.1021/acs.inorgchem.0c02932.

[94] Verweij PD, Driessen WL, Reedijk J, Rowatt B, Sherrington DC. Selective and rapid uptake of copper(II) by a novel chelating resin containing imidazole groups. React Polym 1990;13:83–92. https://doi.org/10.1016/0923-1137(90)90043-4.

[95] Yamauchi O, Tanaka H, Uno T. Studies on imidazole derivatives as chelating agents. I. Syntheses of azoimidazoles and their reactions with metal ions. Chem Pharm Bull 1966;14:948–52. https://doi.org/10.1248/cpb.14.948.

[96] Senapoti S, Sarker KK, Mondal TK, Sinha C. Copper(I) and Silver(I) complexes of 1-alkyl-2-(methyl)-4-(arylazo)imidazole. Synthesis, spectral studies and electrochemistry. Transit Met Chem 2006;31:293–8. https://doi.org/10.1007/s11243-005-6376-1.

[97] Chen W, Chu J, Mutikainen I, Reedijk J, Turpeinen U, Song Y-F. Tripodal bis (imidazole)-based ligands and their chelation to copper(ii). CrystEngComm 2011; 13:7299. https://doi.org/10.1039/c1ce05556a.
[98] Radzyminska-Lenarcik E, Ulewicz M. Application of polymer inclusion and membranes supported with 1-alkyl-2-methylimidazoles for separation of selected transition metal ions. Desalination Water Treat 2017;64:425–31. https://doi.org/10.5004/dwt.2017.11419.
[99] Radzyminska-Lenarcik E, Ulewicz R, Ulewicz M. Zinc recovery from model and waste solutions using polymer inclusion membranes (PIMs) with 1-octyl-4-methylimidazole. Desalination Water Treat 2018;102:211–9. https://doi.org/10.5004/dwt.2018.21826.
[100] Ulewicz M, Sadowska K, Biernat JF. Facilitated transport of Zn(II), Cd(II) and Pb (II) across polymer inclusion membranes doped with imidazole azocrown ethers. Desalination 2007;214:352–64. https://doi.org/10.1016/j.desal.2006.12.006.
[101] Ulewicz M, Sadowska K, Biernat JF. Selective transport of Pb(II) across polymer inclusion membrane using imidazole azocrown ethers as carriers. Physicochem Probl Miner Process 2007;41:133–43.
[102] Fnfoon DY, Al-Adilee KJ. Synthesis and spectral characterization of some metal complexes with new heterocyclic azo imidazole dye ligand and study biological activity as anticancer. J Mol Struct 2023;1271:134089. https://doi.org/10.1016/j.molstruc.2022.134089.
[103] Hasan Mubark HM, Witwit IN, Ali AAM. Synthesis of new azo imidazole ligand and fabricating it's chelate complexes with some metallic ions. J Phys, Conf Ser 2020;1660:012031. https://doi.org/10.1088/1742-6596/1660/1/012031.
[104] Shi S-M, Jiang S-S, Jin C-M. Synthesis, crystal structure and photoisomerization of Co(II)/Cd(II)/Cu(II)/Zn(II) complexes based on arylazoimidazole ligands. J Mol Struct 2025;1335:141988. https://doi.org/10.1016/j.molstruc.2025.141988.
[105] Ebrahimipour SY, Mohamadi M, Castro J, Mollania N, Rudbari HA, Saccá A. Syntheses, characterizations, crystal structures, and biological activities of two new mixed ligand Ni(II) and Cu(II) schiff base complexes. J Coord Chem 2015;68: 632–49. https://doi.org/10.1080/00958972.2014.1000883.